water

MDPI

Supplementary material

Simulation of Heat Flow in a Synthetic Watershed: Lags and Dampening across Multiple Pathways Under a Climate-Forcing Scenario

Daniel T. Feinstein [1,*], Randall J. Hunt [2], and Eric D. Morway [3]

1. U.S. Geological Survey Upper Midwest Water Science Center, 3209 North Maryland Avenue, Milwaukee, WI 53211, USA
2. U.S. Geological Survey Upper Midwest Water Science Center, 1 Gifford Pinchot Drive,Madison, WI 53726, USA
3. U.S. Geological Survey Nevada Water Science Center, 2730 N. Deer Run Road, Carson City, NV 89701, USA

* Correspondence: dtfeinst@usgs.gov

Citation: Feinstein, D.T.; Hunt, R.J.; Morway, E.D. Supplementary Material Sections for Simulation of Heat Flow in a Synthetic Watershed: Lags and Dampening across Multiple Pathways Under a Climate-Forcing Scenario. *Water* **2022**, *14*, 2810. https://doi.org/10.3390/w14182810

Academic Editor: Cristina Di Salvo

Received: 23 June 2022
Accepted: 29 August 2022
Published: 9 September 2022

Section S1—Construction of a Heat Flow Time Series From a High-Emission Climate Scenario

This supplementary material section provides more explanation and detail on how a representative climate scenario was constructed for watershed-scale heat transport modeling. The material here is intended to augment the main article text discussion; however, some main text material is included again here to maintain presentation flow and minimize switching between publications.

The optimal temporal discretization for forcing functions depends on the model objectives. In this study, we are focused on the effects of climate change over a 30-year window in response to a signal subject to seasonal oscillations, long-term trends and random variability. Monthly time steps are assumed to be sufficient to incorporate the seasonal, random and non-stationary aspects of the climate forcing. Because climate change is a transient phenomenon, when modeling the heat inflow subject to climate change, the "warming" period must be preceded by a "spinup" which establishes conditions of dynamic equilibrium at the start of warming. For spinup in this study, the transient forcing function cyclically repeated the average monthly infiltration rates and average monthly infiltration temperatures for 30 years. In effect, the seasonal component of the forcing is realized during the spinup without imposed trend or random variation. For reasonable initial conditions in terms of the dependent variable temperature, the model will settle on a cyclic temperature pattern that is stable at the end of the 30-year spinup. At that point, the infiltration rates and temperatures can vary on a monthly basis reflecting not only the underlying seasonal periodicity, but also random and deterministic trend components.

Figure S1-1. Monthly heat forcing applied to synthetic model during 30-year spinup; a) monthly temperature signal (°C) for spinup, and b) monthly infiltration rate (inch/year) for spinup.

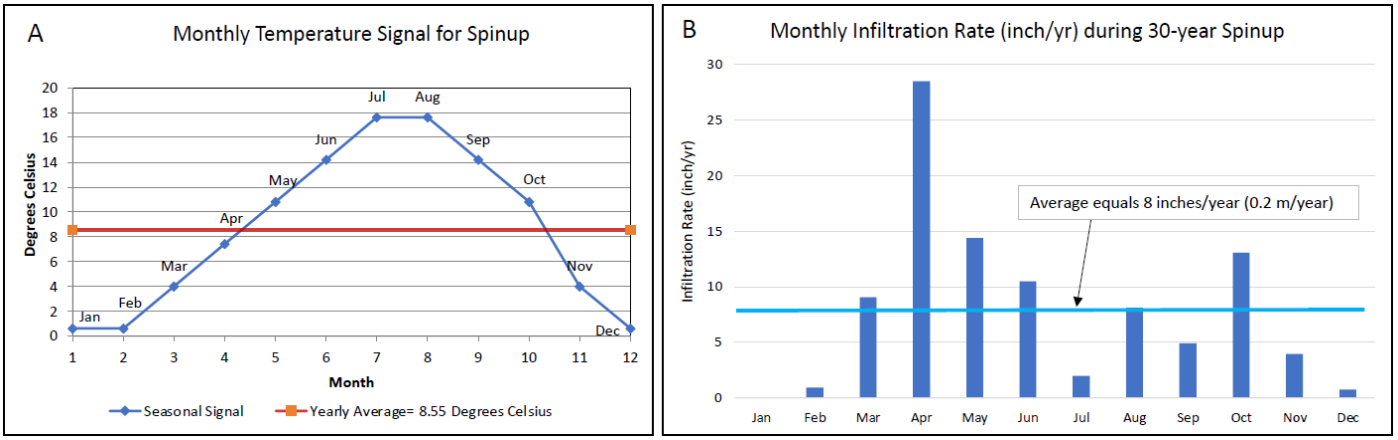

Average monthly temperatures were imposed in a generic fashion. The periodic infiltration rate and temperature forcing applied during spinup are graphed in Figure S1-1a-b. Both time series display a seasonal pattern: the infiltration temperature during spinup is perfectly sinusoidal (moving between a winter minimum of 0.62 °C), and maximum in summer of 17.62 °C corresponding to a cool temperate thermal regime), whereas the infiltration rate forcing is a more complicated wave pattern reflecting mechanisms such as spring snowmelt. The two timeseries are input separately: the infiltration rates are entered into the flow model via the MODFLOW UZF package (Niswonger et al., 2006), whereas the infiltration temperatures are entered into the linked transport model via the MT3D-USGS UZT package (Bedekar et al., 2016). However, they must be taken jointly to define the transient heat inflow imposed on the system.

One way to express the combined forcing is by calculating a *relative heat inflow* time series as a ratio of the product for the two values in a given month to the product of their global averages over the entire spinup period. The ratio of course is indifferent to the units assigned the underlying time series as they cancel. The resulting time series for relative heat inflow is shown on the left side of Figure S1-2—the first 30 years of the plot correspond to spinup and is strictly periodic. The average ratio value across the spinup is, by design, exactly 1.0.

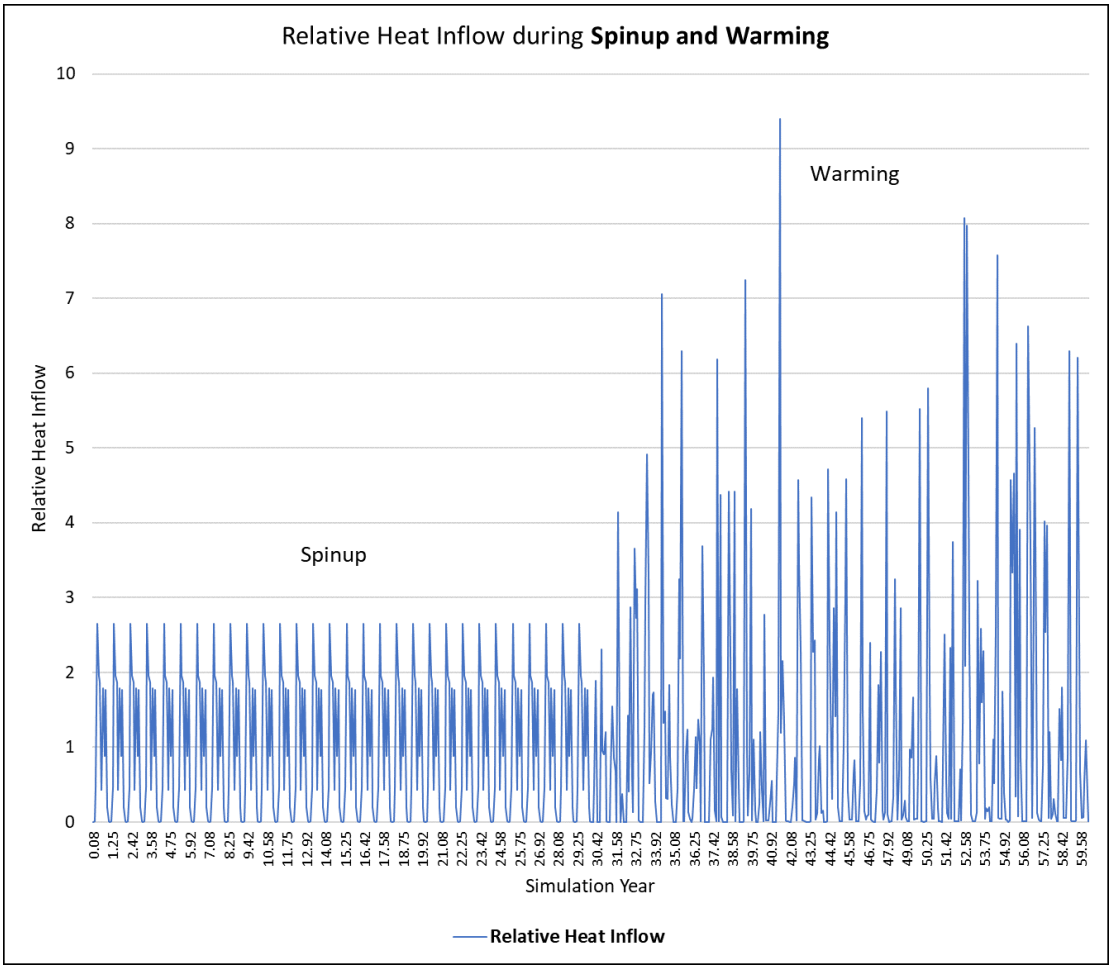

Figure S1-2. Relative heat inflow applied to synthetic model during spinup and warming periods showing temperature signal subjected to cumulative 2 degree C linear increase during warming; infiltration rate subject to cumulative 0.25 inch/year linear increase during warming. Both model versions (MID_TRENDED and HI_TRENDED) subject to same forcing.

The spinup conditions in the current work differ from those imposed in the companion study presented in Morway et al., 2022. The periodic temperature forcing is the same, but whereas in this case the rate forcing at the top of the unsaturated zone (UZ) is variable from month to month, in the companion study the spinup rate was kept constant, set at 8 inch per year (0.2 m per year). The settings for both renditions result in dynamic equilibrium with respect to heat inflow after 30 years of spinup. In the companion study, however, variable monthly infiltration rates are only imposed during the subsequent warming period. This innovation results in a "shock" to the system that promotes much more overall warming than would be attributable to the warming trend alone (set at 0.0025 °C per month, amounting to 0.9 °C over 30 years). The enhanced warming imposed by the onset of rate seasonality after the spinup is useful from a heuristic standpoint—it strengthens the simulated temperature increase at the water table, in the groundwater, and at surface water over the warming period, thereby displaying more clearly the power of the proposed method to capture effects of climate change. The focus of the companion paper is on the presentation of a method for simulating unsaturated/saturated heat transport at the watershed scale, but in this study the objectives are different. We aim here for a more realistic forcing during spinup (by considering variable infiltration rates as well as temperatures on an average monthly basis) so that the effects of subsequent warming are more closely tied to the explicit high-emissions warming trend imposed on the watershed system. In this way, we can generate outputs in the form of energy lags and temperature dampening that more closely reflect expected future warming conditions and, therefore,

that promise to be more useful for drawing lessons to support proper construction of heat-propagation models representing real-world watersheds.

In a general sense, global warming in the upper Midwest of the United States is expected to result in warmer and wetter conditions. Global climate change models (GCM) are designed to produce scenarios for future conditions based on distinct emissions scenarios for CO2. A summary graphs indicating how GCM scenarios forecast global temperature change is reproduced in Figure S1-3. The curves group results from 20 GCM; the five scenarios range from low to high emissions. The high-emission scenario (SSP5-8.5, also referred to as RCP-8.5) is notable because the rate of emission is assumed to increase rather than level off or decrease with time. The temperature curves in Figure S1-3 predict global trends combining terrestrial and ocean response. However, it is possible to downscale the individual and aggregated model results with proper attention to biases and to develop curves for a mosaic of regional watersheds (e.g., used by Hunt et al., 2013; 2016).

For this study, the high-emissions RCP-8.5 climate scenario was selected as the basis for quantifying warming trends in terms of infiltration temperature and infiltration rates. Southern Wisconsin was selected as the down-scaled region to represent temperate climate conditions representative of a temperate climate zone. The selected time frame for projected warming corresponds to 2022 through 2051. This 30-year period is short enough that the forcing predicted by the high emissions scenario show largely linear behavior (Figure S1-3). The U.S. Geological Survey has amassed individual and aggregated GCM results for basins in the United States. (including the HUC7 southern Wisconsin River basin). The atmospheric temperature and precipitation results for individual and aggregated GCM are available online (USGS, 2022).

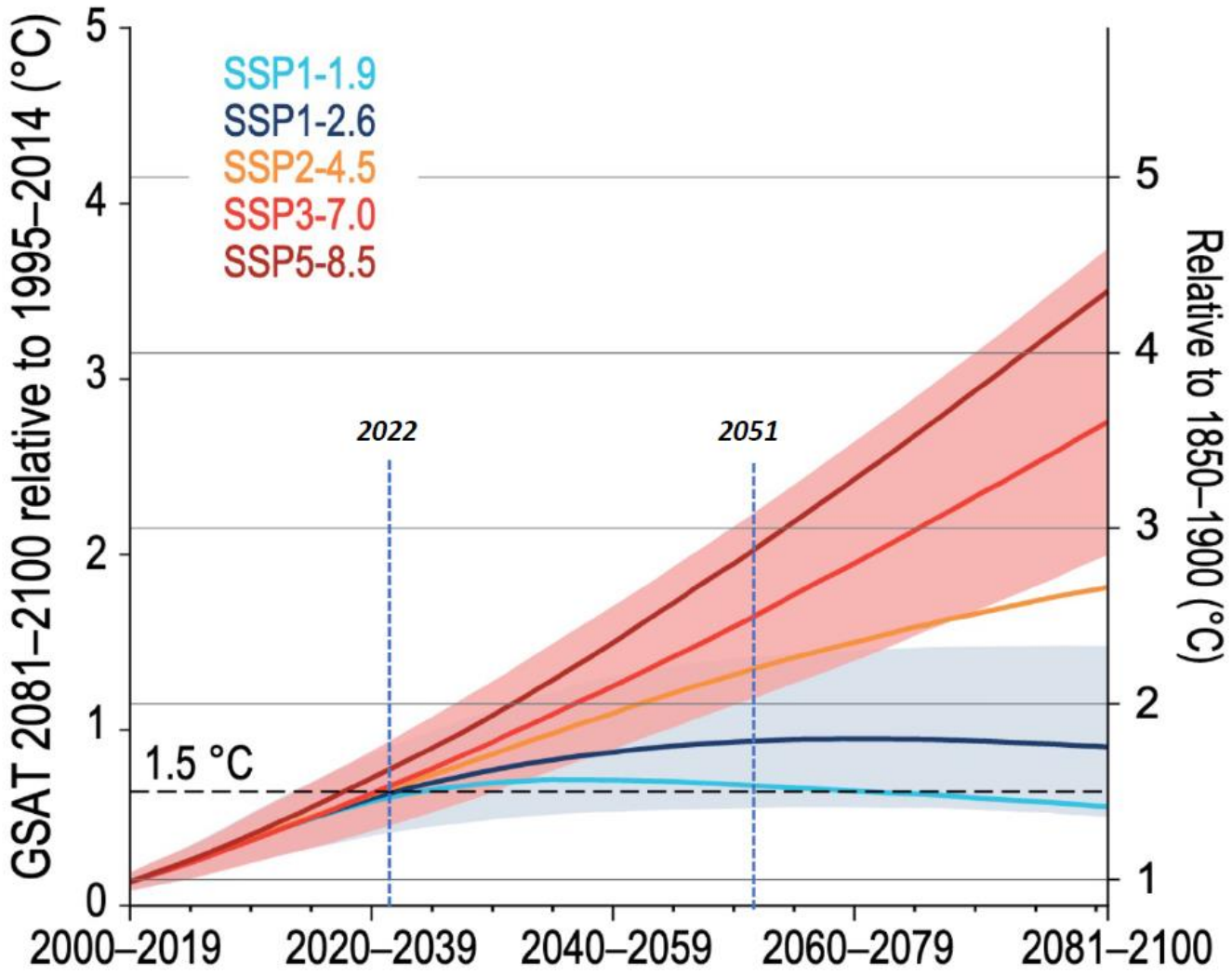

Figure S1-3. RCP scenarios for global temperature changes including RCP8.5 high-emissions scenario, (source https://www.ipcc.ch/report/ar6/wg1/downloads/report/IPCC_AR6_WGI_TS.pdf, accessed 5 February 2022), showing mean temperature rise in set of 20 GCM model highlighted for 2022-2051 period, showing global (rather than down-scaled) scenarios for Representation Concentration Pathways (RCP) scenarios.

One way to display aggregated predictions across the 20 GCM models in the online datasets is through the Mean Model results. Graphs of predicted temperature and precipitation for the selected basin and time frame (Feinstein et al., 2022—Figure 2b-c) display much seasonal and random variability. However, the predicted effect of emissions on warming can be summarized by reducing the time series to a simple linear trend. For the southern Wisconsin River basin, the linear temperature trend yields 0.07 °C rise per year a cumulative 2.1 °C rise over the 30-year span. This result was rounded to 2.0 °C for the purposes of the present study. The precipitation rise is rather modest, equal to 1.0 inch/year (0.025 m/year) after 30 years. For simplicity, the linear trend is applied uniformly without to respect to month or season. Both these trends are input to the hypothetical heat propagation model under study. The atmospheric temperature trend is assumed to hold for the infiltration exiting the root zone at the top of the UZ. The rise in the infiltration rate at the top of the UZ is assumed to be one-quarter of the precipitation rise, amounting to an increase of 0.00833 inches/year (0.00021 m/year) and adding 0.25 inches (0.00635 m) to infiltration after 30 years.

The linear trends are just one component of the infiltration time series applied to the warming portion of the transient flow and transport simulations. Monthly infiltration rate forcing was based on over 30 years from the Black Earth watershed in southern Wisconsin and normalized to an average yearly rate of 8 inch/year supply the seasonal and random components of the time series (Table 1). These values are slightly modified by superimposing the infiltration rate linear trend monthly as described above, producing a 3% increase to an average rate of 8.25 inch/year (0.21 m/year) after 30 years (Feinstein et al., 2022—Figure 2c). The infiltration temperature time series maintains the periodicity from the spinup period (Feinstein et al., 2022—Figure 2b), but random variations are imposed on the sinusoidal signal by sampling from a uniform distribution without autocorrelation varying between -2 and +2 °C. The temperature-warming trend is imposed on the randomized seasonal signal, culminating in about a 2.0 degree rise after 30 years.

As emphasized in Morway et al., 2022, the infiltration rate and infiltration temperature series combine to make heat available to the subsurface. Their joint forcing can be indexed in a relative heat inflow time series, represented in Figure S1-2 for both the spinup and warming periods and in Figure S1-3 for the warming period alone. The heat inflow shows no upward trend during spinup, but a rise is evident by design during warming. The variability from month to month is high, but the cumulative effect of the warming can be distilled by considering the one-year moving average of the time series as well as the overall linear trend in the warming period (Figure S1-3). It is noteworthy that random variations and the cumulative effect of the imposed linear trends on infiltration rate and temperature yield much more increase in the relative heat inflow in the last third of warming than in the preceding 20 years (although, due to random variation, the forcing is weakened somewhat at the very end of the 30-year warming period). It is also important to note that the cumulative linear rise in the relative heat inflow at the end of warming amounts to 1.25 times the equilibrium conditions at the end of spinup 30 years earlier. This value effectively represents the "climate change expectation" in terms of the heat added to the subsurface attributable to wetter and warmer conditions. Most of this increase is due to the assumed infiltration temperature trend; only a small part is due to the assumed infiltration rate trend. By way of comparison, the cumulative value of 1.25 is half the overall 1.5 increase generated by the (exaggerated) forcing conditions presented in the companion article, which focused on the development of the modeling method (Morway et al., 2022).

Any use of trade, firm, or product names is for descriptive purposes only and does not imply endorsement by the U.S. Government.

References

1. Niswonger, R.G.; Prudic, D.E.; Regan, R.S. Documentation of the Unsaturated-Zone Flow (UZF1) Package for modeling Unsaturated Flow Between the Land Surface and the Water Table with MODFLOW-2005. **2006**, https://doi.org/10.3133/tm6a19.
2. Bedekar, V.; Morway, E.D.; Langevin, C.D.; Tonkin, M.J. MT3D-USGS version 1: A U.S. Geological Survey release of MT3DMS updated with new and expanded transport capabilities for use with MODFLOW. **2016**, https://doi.org/10.3133/tm6a53.
3. Morway, E.D.; Feinstein, D.T.; and Hunt, R.J. Simulation of Heat Flow in a Synthetic Watershed: Lags and Dampening across Multiple Pathways under a Climate-Forcing Scenario. *Water*, **2022**, *14*, 2810. https://doi.org/10.3390/w14182810
4. Hunt, R.; Walker, J.F.; Selbig, W.; Westenbroek, S.M.; Regan, R.S. . Simulation of climate-change effects on streamflow, lake water budgets, and stream temperatures using GSFLOW and SNTEMP, Trout Lake Watershed, Wisconsin, U.S. Geological Survey Scientific Investigations Report 2013-5159, 118 p., http://pubs.usgs.gov/sir/2013/5159/.
5. Hunt, R.J.; Westenbroek, S.M.; Walker, J.F.; Selbig, W.R.; Regan, R.S.; Leaf, A.T.; Saad, D.A. Simulation of climate change effects on streamflow, groundwater, and stream temperature using GSFLOW and SNTEMP in the Black Earth Creek Watershed, Wisconsin. **2016**, 1–117, https://doi.org/10.3133/sir20165091.
6. United States Geological Survey, 2022, National Climate Viewer. Available online:https://www2.usgs.gov/landresources/lcs/nccv/maca2/maca2_watersheds.html (accessed on 2 September 2022).
7. Feinstein, D.T.; Hunt, R.J.; Morway, E.D. Simulation of Heat Flow in a Synthetic Watershed: Lags and Dampening across Multiple Pathways under a Climate-Forcing Scenario. *Water* **2022**, *14*, 2810, https://doi.org/10.3390/w14182810.

Section S2—Additional Model Construction Information

This Appendix provides more explanation and detail on how the synthetic model was constructed for watershed-scale heat transport simulations using MODFLOW-NWT (Niswonger et al., 2011) and MT3D-USGS (Bedekar et al., 2016). The material here is intended to augment the main article text discussion; however, some main text material is included again here to maintain presentation flow.

The synthetic model construction is identical in terms of geometry, parameter values, and boundary conditions to what is presented in Morway et al., 2022. The design is characterized by:

- a transient climate forcing function which combines transient infiltration rates and transient infiltration temperatures into a single time-dependent heat inflow function (recharge is time dependent);
- spatially uniform application of climate forcing across the model domain (recharge is spatially uniform);
- spatially uniform flow and transport parameters across the model domain.

Planview elements of the model are shown in Figure S2-1. The lateral grid spacing is uniform, with cells 91 m (300 feet) on a side. The grid consists of 300 columns and 300 rows, yielding a domain area corresponding to the dimensions of a HUC10-category watershed. They include model sinks in the form of streams, wetlands, and a lake, represented by the MODFLOW SFR, DRN and LAK packages respectively; collectively, these features cover about 13% of the model domain. A boundary line of inlet cells at the northern edge of the model and a boundary line of outlet cells at the southern edge of the mode are represented by the GHB package. The remaining model perimeters are no-flow boundaries.

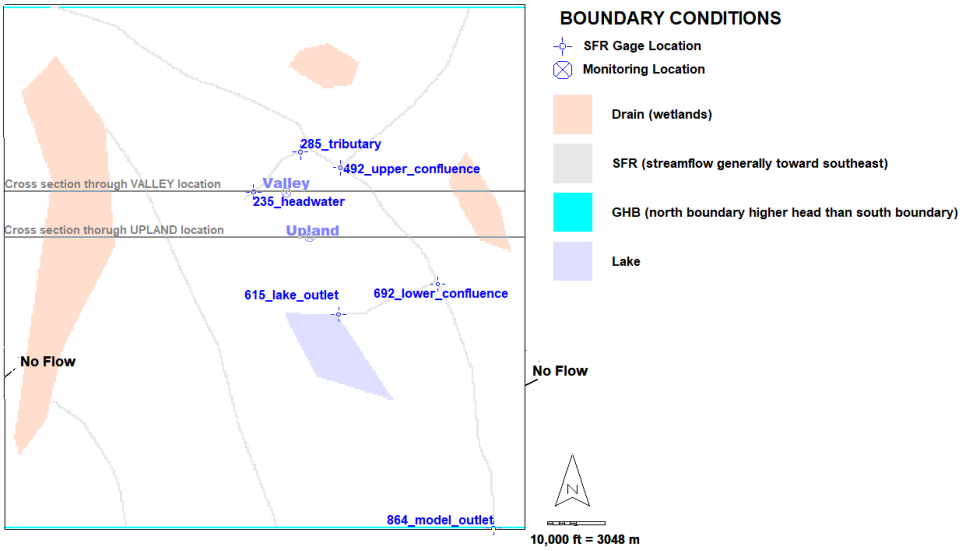

Figure S2-1. Synthetic model setup showing domain and boundary conditions, as well as locations for monitoring temperature results. Cross-sections are shown in Figure 2. SFR = Stream Flow Routing; GHB = General Head Boundary.

The model layering is shown in Figure S2-2 (the two versions are discussed below). An important aspect of the vertical discretization is the presence of a 0.9-m (3-foot) thick "receptor" layer at the surface that conveys infiltration from the land surface to the top of the unsaturated zone (UZ). It notionally fills the volume occupied by the root zone, but the applied infiltration is net of the evapotranspiration that occurs in the root zone, such that the actual top of the model corresponds to the zero-flux boundary at the bottom of the root zone where water and heat flow begin to move downward toward the water table.

Cells in the receptor layer (i.e., layer 1) are typically unsaturated, but they can host the water table in riparian zones near surface-water features. They can also receive discharge to the land surface in the form of seepage (see discussion of UZF functionality in Morway et al., 2022). Cells in layers 2 through 4 below the receptor layer can be either unsaturated, partially saturated (that is, host the water table), or fully saturated and the condition can change by stress period. Layers 5 through 8 are always fully saturated and transmit groundwater flow toward surface-water discharge features.

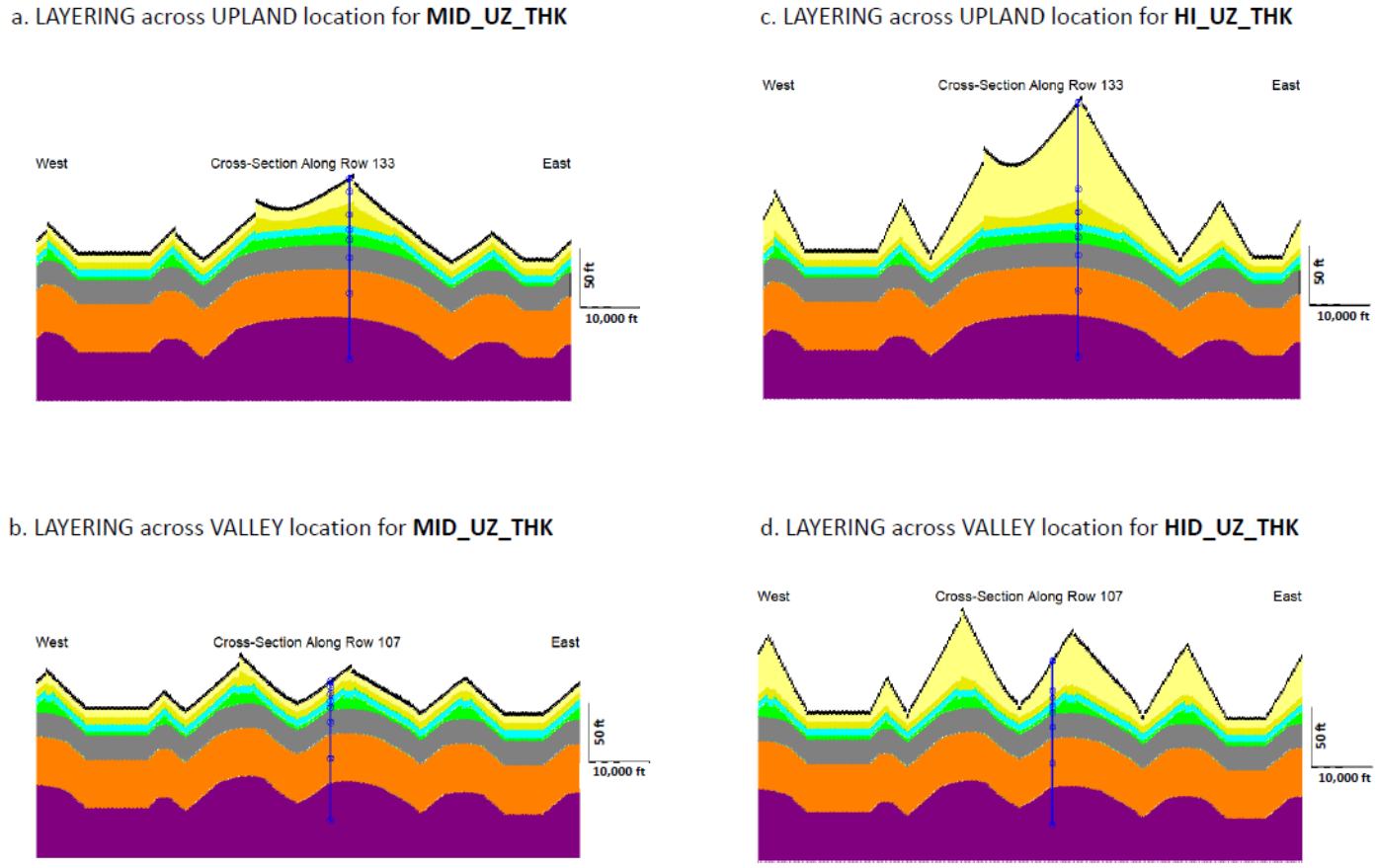

Figure S2-2. Layering through UPLAND and VALLEY locations; a) MID_UZ_THK, UPLAND cross section. b) MID_UZ_THK, VALLEY cross section. c) HI_UZ_THK, UPLAND cross section. d) HI_UZ_THK, VALLEY cross section. Cross section locations are shown in Figure S1-1. Top black layer is 3-ft thick receptor layer for receiving infiltration.

Parameter values for the flow and transport simulations are listed in Tables S2-1 and S2-2.

Table S2-1 MODFLOW-NWT groundwater flow model parameters

A. Subsurface Parameters	**Value (English length units)**	**Value (Metric length units)**
SAT horizontal hydraulic conductivity	42.5 ft/day	12.95 m/day
SAT vertical hydraulic conductivity	1.0 ft/day	0.30 m/day
Vertical UZ hydraulic conductivity	1.0 ft/day	0.30 m/day
UZ SURFK	0.10 ft/day	0.0305 m/day
SAT specific yield	0.26 (--)	0.26 (--)
SAT specific storage	$1x10^{-5}$ 1/day	$3.289x10^{-5}$ 1/day
UZ saturated water content	0.30 (--)	0.30 (--)
UZ residual water content	0.04 (--)	0.04 (--)
UZ Brooks-Corey epsilon	3.87 (--)	3.87 (--)
UZ monthly infiltration rate	see Figure S1-1	

B. Boundary Condition Parameters *	**Value (English length units)**	**Value (Metric length units)**
Stream (SFR) channel width	25 ft	7.62 m
Stream (SFR) bed thickness	1 ft	0.30 m
Stream (SFR) bed vertical hydraulic conductivity	20 ft/day	6.10 m/day
Stream (SFR) channel slope	0.0002 (--)	0.0002 (--)
Stream (SFR) top of streambed	2.5 ft below land surface	0.76 m below land surface
Wetland (DRN) bed conductance	90,000 ft^2/day	8361 m^2/day
Wetland (DRN) stage	Western= 275 ft above datum Northern= 285 ft above datum Eastern= 270 ft above datum	Western= 83.8 m above datum Northern= 86.9 m above datum Eastern= 82.3 m above datum
Lake (LAK) bed conductance	90,000 ft^2/day	8361 m^2/day
Lake (LAK) initial stage (model resolves stage with time)	268 ft above datum	81.7 m above datum
Lake (LAK) precipitation	32 inch/year	0.81 m/year
Lake (LAK) evaporation	-32 inch/year	-0.81 m/year
Northern and southern boundary (GHB) conductance	11.3636 ft^2/day	1.05573 m^2/day
Head difference (GHB) between northern and southern boundary	69.684 ft	21.24 m
Heat gradient (GHB) between northern and southern boundary	0.00078 (--)	0.00078 (--)
Lake (LAK) bed conductance	90,000 ft^2/day	8361 m^2/day
Lake (LAK) initial stage (model resolves stage with time)	268 ft above datum	81.7 m above datum
Lake (LAK) precipitation	32 inch/year	0.81 m/year
Lake (LAK) evaporation	-32 inch/year	-0.81 m/year
Northern and southern boundary (GHB) conductance	11.3636 ft^2/day	1.05573 m^2/day
Head difference (GHB) between northern and southern boundary	69.684 ft	21.24 m
Heat gradient (GHB) between northern and southern boundary	0.00078 (--)	0.00078 (--)

*Stream (SFR) channel lengths per cell are variable, depending on network geometry
Note: UZ=unsaturated zone; SAT=saturated zone,
MODFLOW boundary packages: SFR= Stream Routing, DRN= Drain, LAK= Lake, GHB= General Head Boundary

Table S2-2. MT3D-USGS transport model parameters.

MT3D-USGS package: Parameter	Value (English length units)	Value (Metric length units)
BTN:		
Porosity	0.3 (--)	0.3 (--)
DSP, for bulk thermal conductivity and bulk thermal diffusion		
Saturated thermal conductivity	52,669 Joules*day^{-1}*ft^{-1}*^{o}C^{-1}	2.0 Joules Joules*sec^{-1}*m^{-1}*^{o}C^{-1}
Residual thermal conductivity	13,167 Joules*day^{-1}*ft^{-1}* ^{o}C $^{-1}$	0.5 Joules*sec-1*m^{-1}* ^{o}C $^{-1}$
Fluid density	28.3166 kg/ft^3	1000 kg/m^3
Fluid heat capacity	4183 joules/kg/ ^{o}C	4183 joules/kg/ ^{o}C
Residual water content	0.04 (--)	0.04 (--)
DSP, for calculation of hydrodynamic dispersion		
longitudinal dispersivity	3.0 ft	0.91 m
transverse horizontal dispersivity	0.30 ft	0.091 m
transverse vertical dispersivity	0.30 ft	0.091 m
UZT:		
Monthly infiltration temperature	see Figure S1-2	
RCT, for sorption:		
Bulk density of solid	51.849 kg/ft^3	1830 kg/m^3
Distribution coefficient	2.68x10^{-3} ft^3/kg	7.59x10^{-5} m^3/kg
SSM, for GHB cells:		
Source temperature	Set to 8.55 ^{o}C during Spinup. added 0.03 ^{o}C /year during Warming	
from SFT		
Initial temperature in all reaches	8.55 ^{o}C	8.55 ^{o}C
from LKT		
Initial lake temperature	8.55 ^{o}C	8.55 ^{o}C
Precipitation temperature	temperature same as infiltration except for following months: Apr: +0.5 ^{o}C, May: +1.0 ^{o}C, Jun: +1 .5 ^{o}C, Jul: +2.0 ^{o}C, Aug: +1.5 ^{o}C, Sep: +1.0 ^{o}C, Oct: +0.5 ^{o}C	

The individual contributing basins associated with stream segments are mapped in Figure S2-3a; nested topographic basins associated with stream gage locations are mapped in Figure S2-3b. The former basins are used to calculate storm runoff inputs to the model, the latter are used to analyze output in terms of heat fluxes and flows.

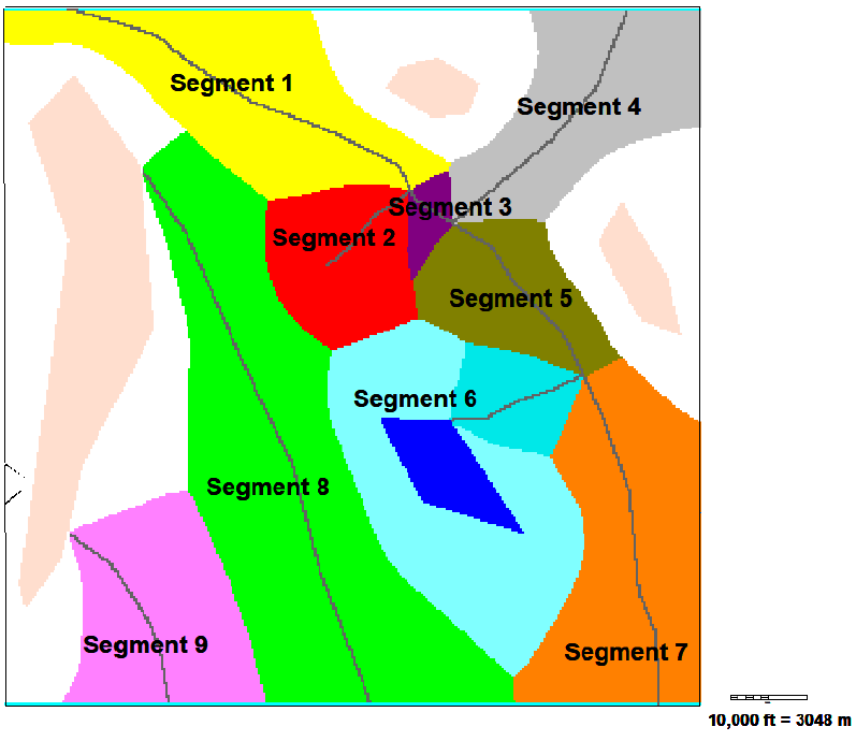

Figure S2-3. a) Stream segment topographic basins corresponding to storm runoff areas.

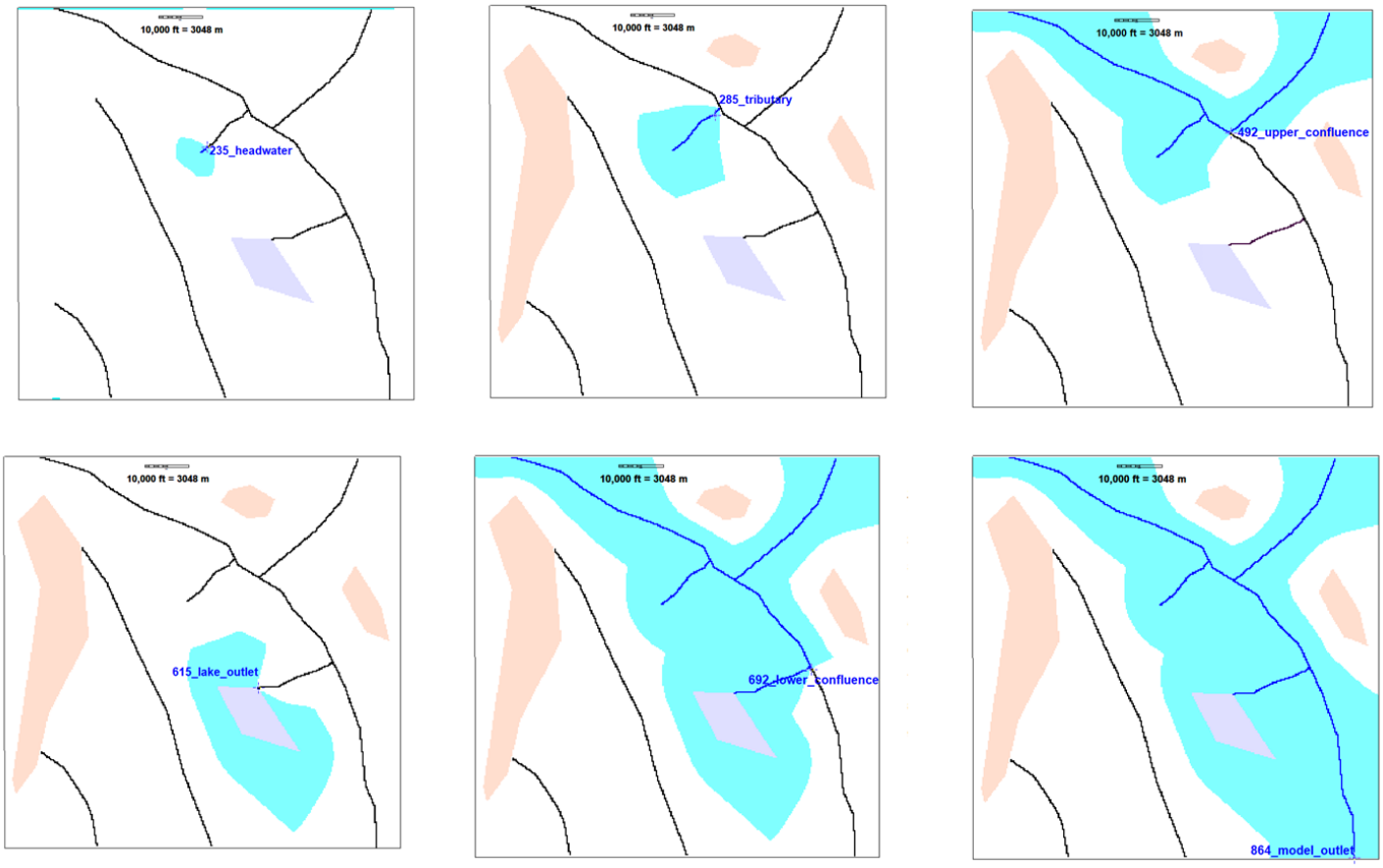

Figure S2-3. b): Nested topographic basins corresponding to gage contributing areas for gages 235 (headwater), 285 (tributary), 492 (upper confluence), 615 (lake outlet), 692 (lower confluence) and 864 (model outlet).

Each transient stress period in the flow and transport simulations has duration of one month. There are 360 stress periods over 30 years during spinup and the same number during warming. The updated forcing functions described in the previous section are applied to the flow and transport models in order to simulate temperatures and energy flows through time and space. Of special interest is the effect of UZ thickness on these results. In the present study two versions of the model are presented to explore the control exercised by the UZ:

8. **MID_TRENDED** (Figure S2-2a-b): this version is designed to produce, on average, a moderate depth to the water table (that is, a moderate UZ thickness). The land surface slopes gradually up from surface-water features. The water-table depth varies from zero feet in riparian areas (commonly about 20% of the model domain) to about 15 m (50 feet) in upland areas.
9. **HI_TRENDED** (Figure S2-2c-d): this version is designed to produce, on average zone, a large depth to water table (that is, a high UZ thickness given temperate climate conditions). The land surface slopes steeply up from surface-water features. The depth varies from zero feet in riparian areas (commonly about 4% of the model domain) to over a 30 m (100) ft in upland areas.

The transient head response to the monthly variations in infiltration at the UPLAND and VALLEY locations is shown at increasing depth (Figure S2-4).

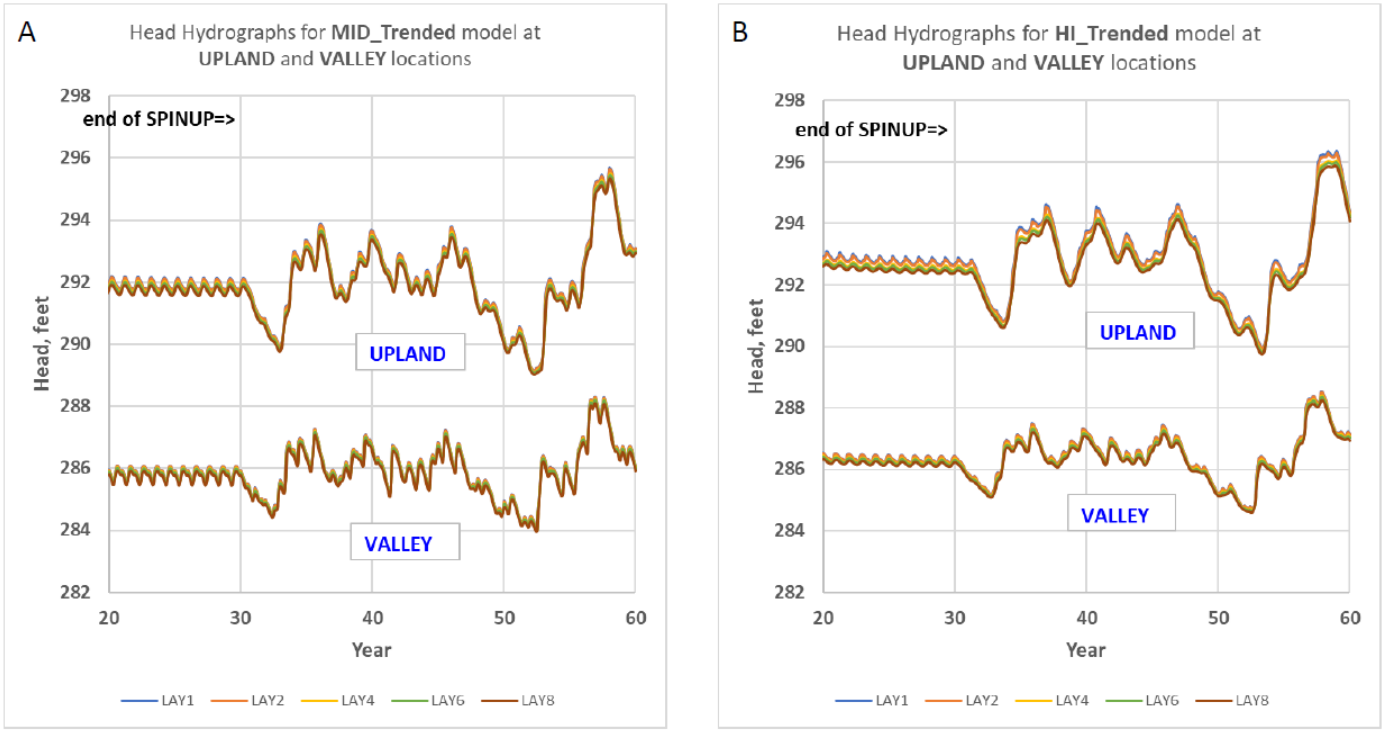

Figure S2-4. Head hydrographs across layers at UPLAND and VALLEY locations for MID_TRENDED (a) and HI-TRENDED (b) model versions.

The two model versions display similar trends, but the generally thicker UZ in the **HI_TRENDED** case yields a smoother head response that is slightly more lagged with respect to the onset of the warming period followed by slightly greater downward head difference between the unsaturated layers. A visualization of the shallow flow field at the end of spinup for the two model versions can be generated (Figure S2-5) and the local groundwater contributing basins to streams, lake and wetlands. More information on model construction and model versions is given in the companion article, Morway et al., 2022.

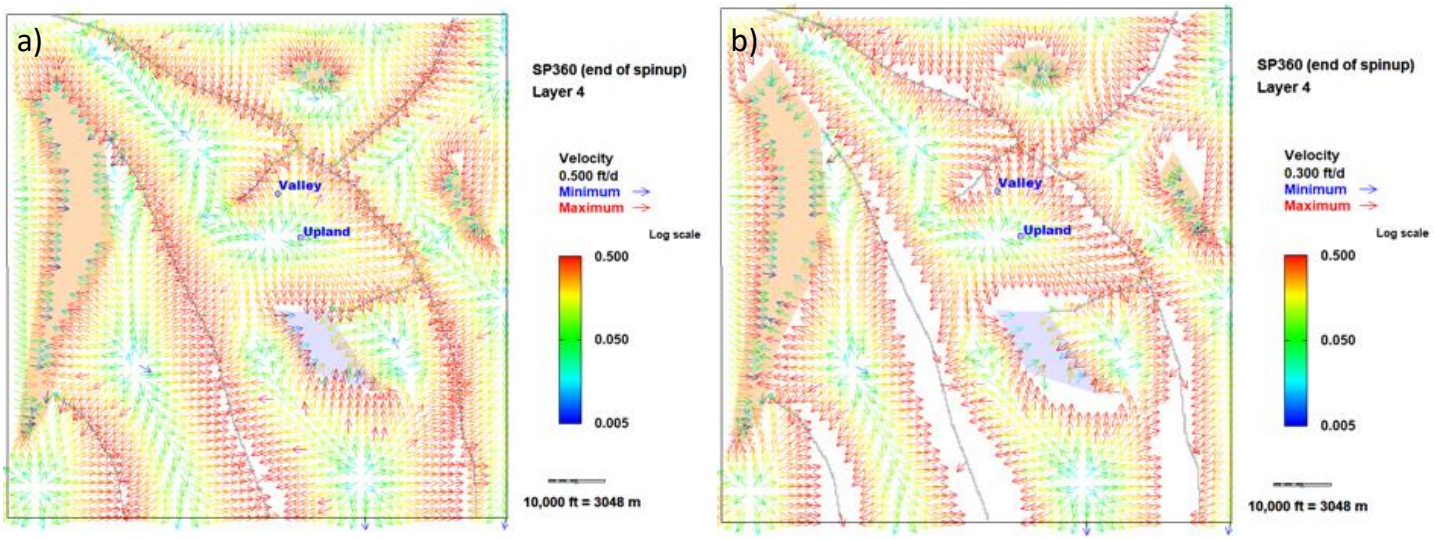

Figure S2-5. Velocity vectors representing synthetic model flow field for the MID_TRENDED (a) and HI-TRENDED (b) cases. Velocities > 0.5 ft/d in white areas.

The new element in model construction is storm runoff, input by taking advantage of options available in the MODFLOW SFR package and the MT3D-USGS SFT package. A simple set of proportions coordinates the storm runoff with other elements of the overall watershed budget—precipitation, evapotranspiration, and the imposed infiltration time series. For the purposes of this exercise, the monthly precipitation (in units of L/T) is assumed equal to four times the monthly infiltration rate for both the spinup and warming periods. Evapotranspiration from the land surface and root zone is assumed equal to two-thirds of monthly precipitation. Storm runoff is the residual term, equal to 1/12th the precipitation rate, or, equivalently, one third the infiltration rate. These ratios are intended to mimic conditions in a sandy watershed where infiltration through the root zone is several times greater than storm runoff. Figure S2-6 shows the budget fluxes for a contributing basin corresponding to the most upgradient stretch of stream on the east side of the synthetic model. The graphed storm runoff values are computed by multiplying the monthly infiltration rates first by 1/3 and then by the basin area (the entire basin is assumed to contribute to runoff). The resulting overland flux is distributed over the draining segment as a function of the stream length in each model cell. The storm runoff flux in other contributing basins follows the same pattern, scaled by their corresponding basin areas, and by again invoking the basic assumption of spatial uniformity of surface as well as subsurface properties across the synthetic model.

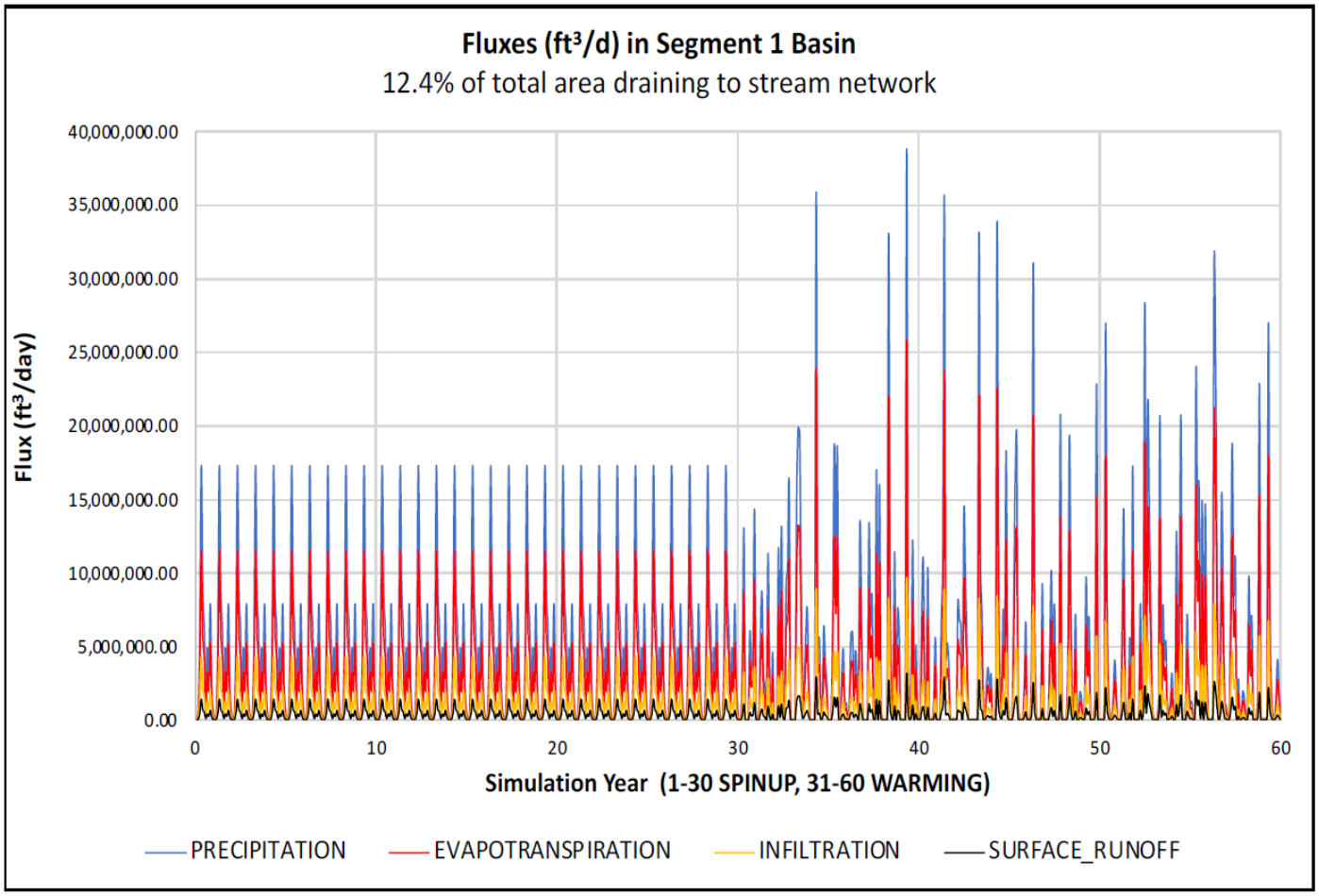

Figure S2-6. Storm runoff logic and budget flux terms for the basin showing specified relation of precipitation, evapotranspiration and storm runoff to the infiltration rate during spinup and warming periods. The absolute fluxes correspond to amounts of an example stream segment.

Storm runoff is also applied to the lake from its contributing basin, which joins with the basin of its outlet stream to add flux to the surface network. Precipitation, set equal to four times the monthly infiltration rate, is also applied directly to the area of the lake surface. The temperature in lake precipitation is equated with monthly infiltration temperatures plus a solar radiation term in the form of an added temperature boost of as much as 2 degrees in the warmer months (see Table S2-2). Neither precipitation nor solar radiation has been added to the stream input, a simplifying assumption that could be replaced by explicit processes in a real-world application.

Note that whereas storm runoff becomes stream stormflow, groundwater runoff, in the form of rejected infiltration plus groundwater discharge to the riparian zone (Feinstein et al., 2022 Figure 1) combines with direct groundwater discharge at the stream channel to generate stream baseflow. The sum of all these fluxes is equal to total streamflow.

The imposed infiltration, representing three-quarters of the water and heat inflow, routes through subsurface pathways. Storm runoff, representing one-quarter of the inflow, is assumed to move instantaneously, at the monthly model time step, from contributing basin to stream segment. The heat in the baseflow portion of total streamflow is derived from infiltration and is subject to phase and amplitude shifts; the heat flow in streams derived from storm runoff is not subject to lags or dampening.

Any use of trade, firm, or product names is for descriptive purposes only and does not imply endorsement by the U.S. Government.

References

1. Bedekar, V.; Morway, E.D.; Langevin, C.D.; Tonkin, M.J. MT3D-USGS version 1: A U.S. Geological Survey release of MT3DMS updated with new and expanded transport capabilities for use with MODFLOW. **2016**, https://doi.org/10.3133/tm6a53.
2. Niswonger, R.G.; Panday, S.; Ibaraki, M. MODFLOW-NWT, A Newton formulation for MODFLOW-2005. **2011**, https://doi.org/10.3133/tm6a37.
3. Morway, E.D., D.T. Feinstein, and R.J. Hunt, 2022. Simulation of heat flow in a synthetic watershed: The role of the unsaturated zone, Journal of Water (In Press)
4. Feinstein, D.T.; Hunt, R.J.; Morway, E.D. Simulation of Heat Flow in a Synthetic Watershed: Lags and Dampening across Multiple Pathways under a Climate-Forcing Scenario. *Water* **2022**, *14*, 2810, https://doi.org/10.3390/w14182810.

Section S3—Additional Information Regarding Simulation Results

This Appendix provides more explanation and detail on results of the watershed-scale heat transport. The material here is intended to augment the main article text discussion; however, some main text material is included again here to maintain presentation flow and minimize switching between publications.

Simulation Results: Temperature trends along pathways

The method under study (Morway et al., 2022) produces time series of simulated temperature in response to climate forcing for various locations, including at the water table, in the groundwater system, and along the surface water network. As discussed in Supplemental Information Appendix S3, the simulated water table typically resides in model layer 4 at the UPLAND location and in model layer 3 at the VALLEY location; shallower layers are unsaturated and the deeper layers are fully saturated. The average temperature during the spinup period is 8.55 °C, however this value does not fully reflect the flux-weighted average temperature that drives heat propagation. When monthly temperatures are weighted by monthly infiltration rates, the effective average temperature during spinup is 9.97 °C, which also applies to storm runoff. The integrated response of the watershed to the spinup forcing is evident in the surface-water temperatures at the end of spinup—stream reaches and the lake all converge to about 10 °C for both the MID_TRENDED and HI_TRENDED simulations. These dynamic equilibrium conditions are disrupted during the 30 years of gradually rising temperatures assigned equally to infiltration and storm runoff. The flux-weighted average forcing temperature for the entire 30-year warming period is 10.95 °C; for the final 10 years of warming, it is 12.23 °C, a 2.26 °C rise relative to the corresponding dynamic equilibrium value during spinup.

Temperature time series generated by the synthetic model (Figure S3-1) show that temperature fluctuations are greatest in the unsaturated layers and are muted in deep saturated layers at both locations. The response is flashier and of higher magnitude where the unsaturated zone (UZ) thickness is smaller, evident from comparison of the MID_TRENDED to HI_TRENDED version results on the one hand, and from the VALLEY to UPLAND location results on the other.

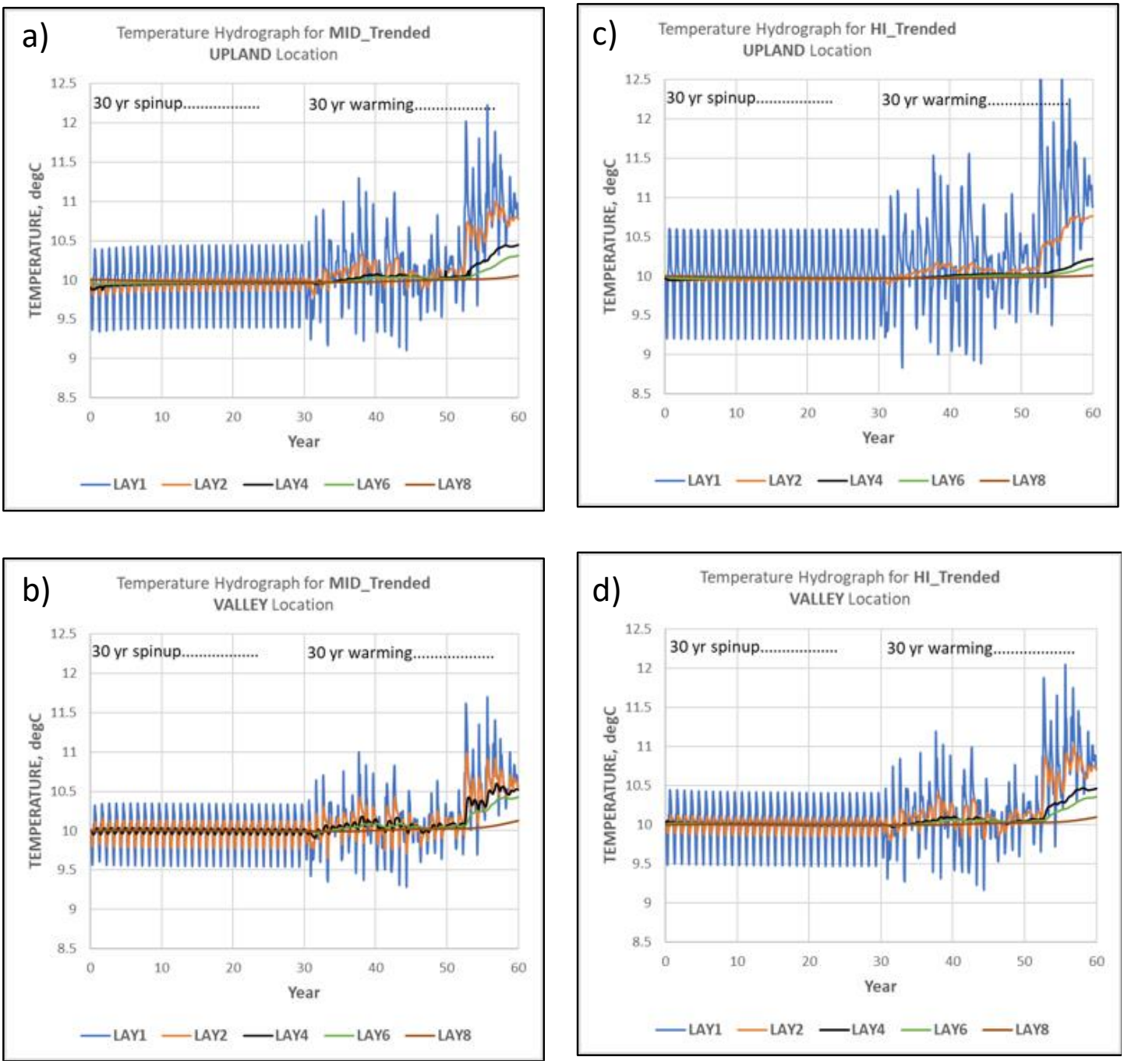

Figure S3-1. Simulated temperature hydrographs (°C) by model layer at UPLAND and VALLEY locations during spinup and warming periods for the MID-TRENDED (a,b) and HI-TRENDED (c,d) cases.

It is instructive to focus on the temperature response at the water table for the two model versions and at the two selected locations (Figure S3-2). (Refer to the cross sections in Figure S2- 2 in Supplemental Information Appendix S2 for the contrasting depths in each case—in each cross section the water table generally falls in layer 4, colored blue). The UZ thickness exercises a strong control on the amplitude and frequency of the temperature time series during warming. At the UPLAND location, the water-table temperature series is smooth and muted for both model versions, largely reflecting the overall warming trend, with some sensitivity to year-by-year fluctuations in the MID_TRENDED results. At the VALLEY location, the depth contrast between the two model versions exercises a stronger control on frequency behavior. Temperatures generated by the

MID_TRENDED for a water-table depth averaging 11 ft (3.3 m) display much spikier behavior than the corresponding **HI_TRENDED** time series at a depth averaging 31 m (9.6 m).

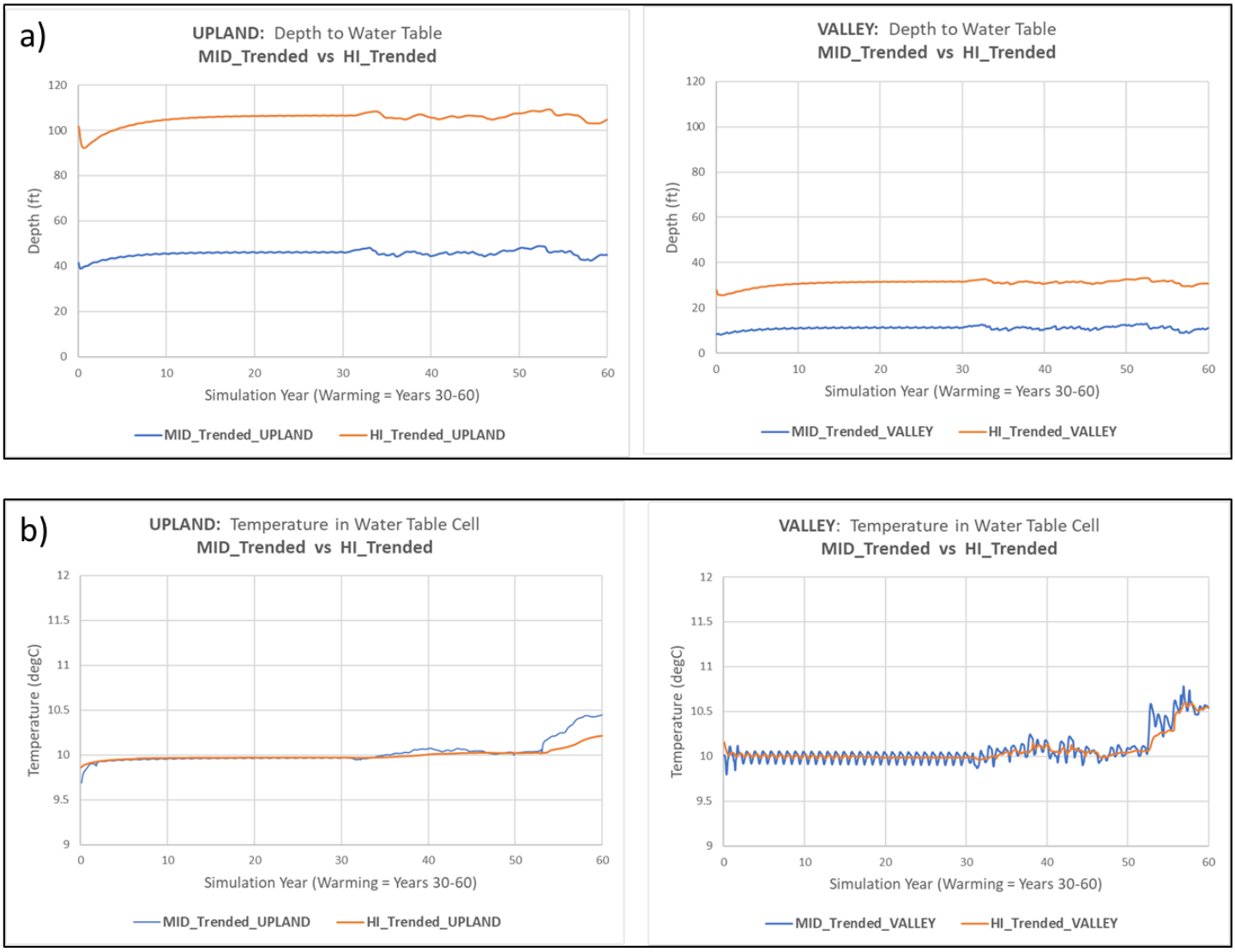

Figure S3-2. Time-series results for Synthetic Model at Upland and Valley Locations: (a) Depth to water table for MID_TRENDED and HI_TRENDED simulations; (b) Water table temperature for MID_TRENDED and HI_TRENDED simulations. Upland and Valley locations are shown in Figure S2-1.

The MID_TRENDED simulation consistently shows a flashier water-table response than does the HI_TRENDED simulation. The temperature response in the surface-water network to seasonality and warming is markedly different from the response in the UZ, at the water table, and in the groundwater system. One way to characterize the stream temperature regime is in terms of the temperature excursion (maximum minus minimum) in total streamflow (runoff plus discharge) during the 30 years of simulated warming. For the gage locations shown in Figure S2-3 in Supplemental Information Appendix S2, the temperature excursion at upstream locations averages about 8.5 °C for both the MID_TRENDED and HI_TRENDED versions of the model (Figure S3-3a and S3-3c; for downstream gages the average is about 7.3 °C (Figure S3-3b and S3-3d). An exception to this simulated pattern is the gage at the lake outlet: it registers a smaller excursion due to the inertial effects of the large volume of lake water.

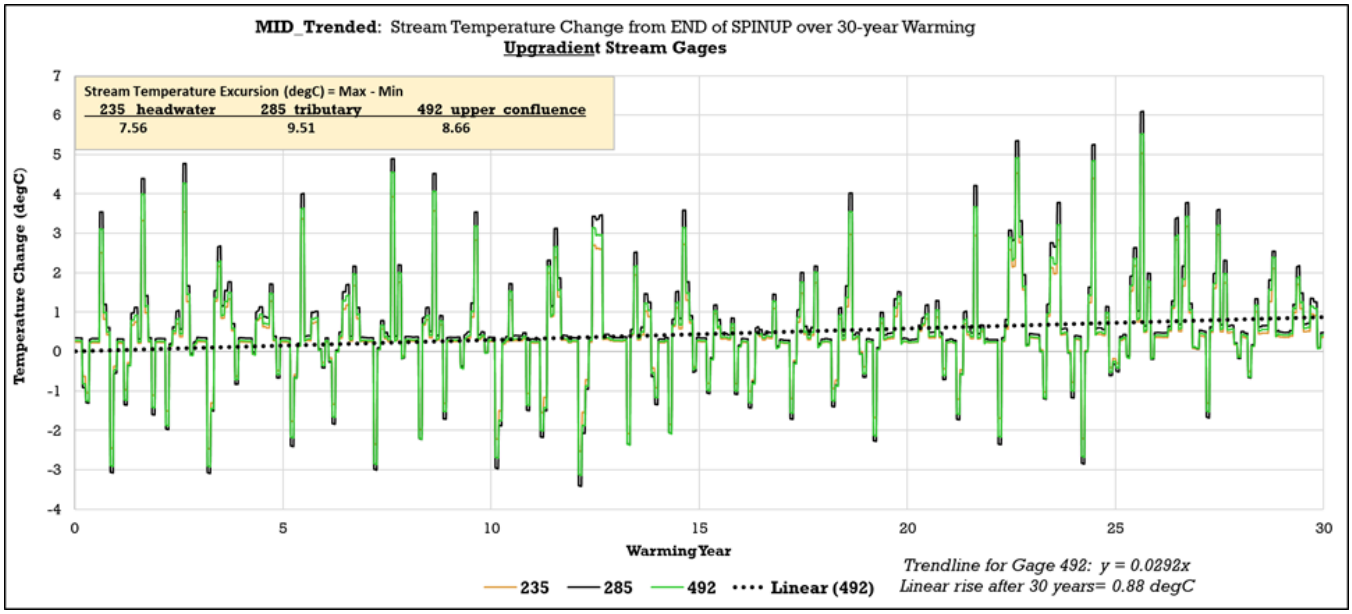

Figure S3-3. a: Changes in stream temperatures (°C) at upstream gages Headwater (235), Tributary (285), and Upper Confluence (492) over warming period relative to end of spinup at gage locations for MID_TRENDED simulation. Linear trend fitted to stream temperatures over warming for Gage 492; Table shows simulated stream temperatures at end of spinup. See Figure S2-3b in Supplemental Information Appendix S2 for gage locations.

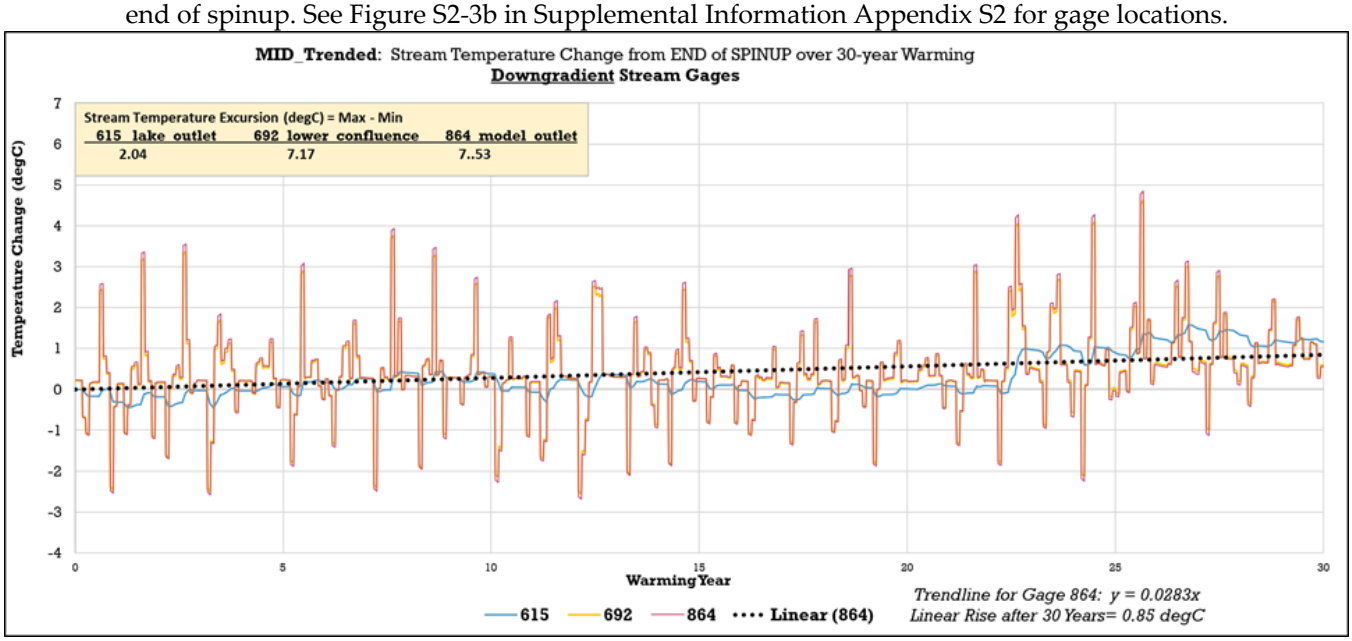

Figure S3-3. b: Changes in stream temperatures (°C) at downstream gages Lake Outlet (615), Lower Confluence (692) and Model Outlet (864) over warming period relative to end of spinup at gage locations for MID_TRENDED simulation. Linear trend fitted to stream temperatures over warming for Gage 864; Table shows simulated stream temperatures at end of spinup. See Figure S2-3b in Supplemental Information Appendix S2 for gage locations.

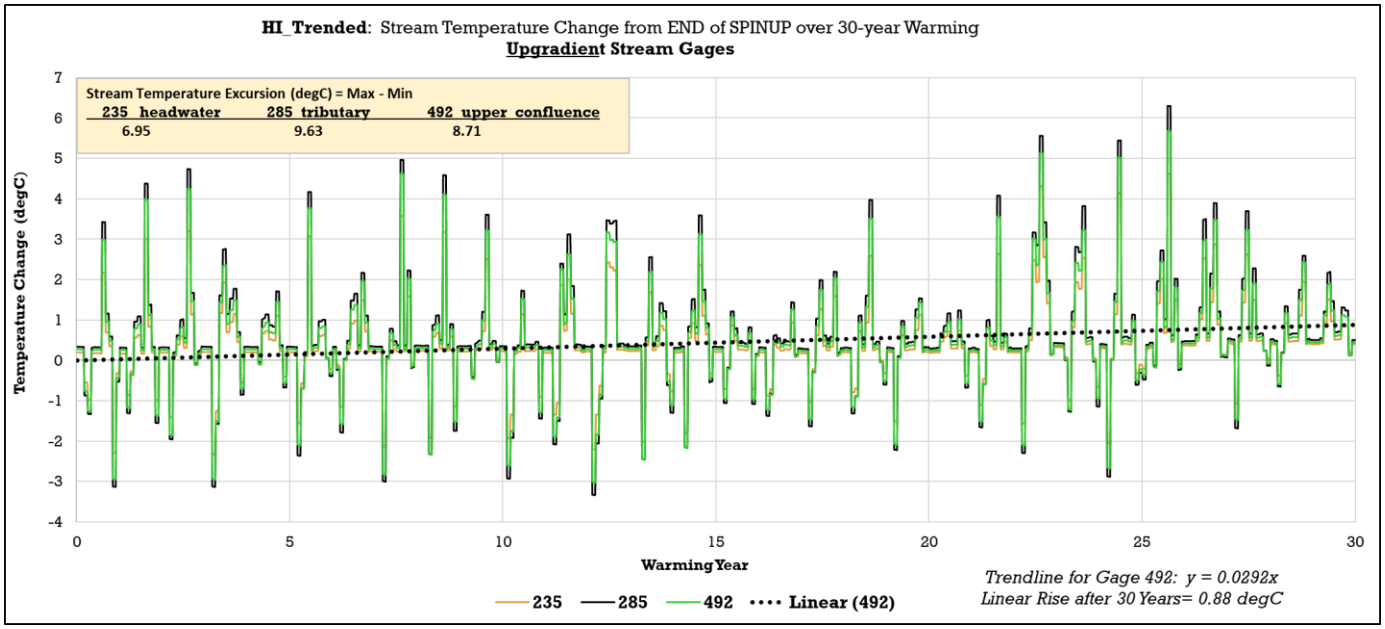

Figure S3-3. c: Changes in stream temperatures (°C) at upstream gages Headwater (235), Tributary (285), and Upper Confluence (492) over warming period relative to end of spinup at gage locations for HI_TRENDED simulation. Linear trend fitted to stream temperatures over warming for Gage 492; Table shows simulated stream temperatures at end of spinup. See Figure S2-3b in Supplemental Information Appendix S2 for gage locations.

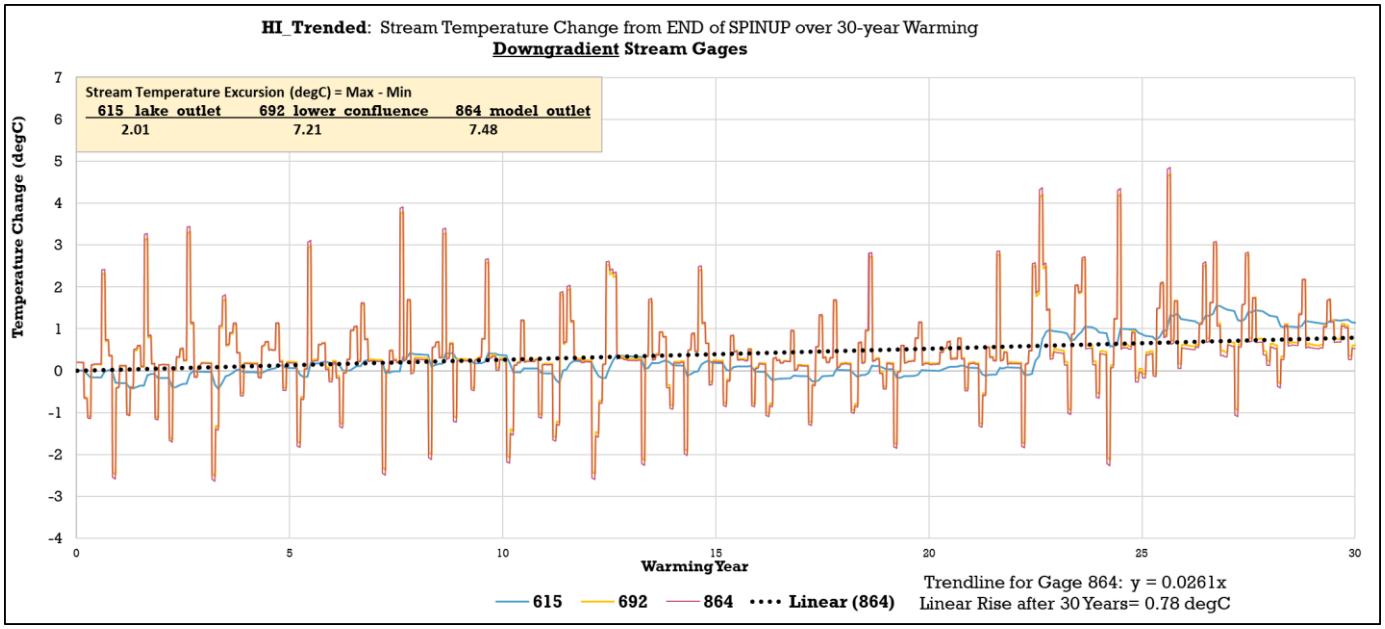

Figure S3-3. d: Changes in stream temperatures (°C) at downstream gages Lake Outlet (615), Lower Confluence (692) and Model Outlet (864) over warming period relative to end of spinup at gage locations for HI_TRENDED simulation. Linear trend fitted to stream temperatures over warming for Gage 864; Table shows simulated stream temperatures at end of spinup. See Figure S2-3b in Supplemental Information Appendix S2 for gage locations.

The size of the temperature excursion in total streamflow reflects the influence of the heat in storm runoff, which during warm, wet months is conveyed rapidly (in the model context, instantaneously) to draining stream segments. Storm runoff constitutes only one-quarter of streamflow in these simulations, but its thermal effect is disproportionally large due to the absence of any lag or dampening effects on its heat load. The storm runoff effect

dwarfs the fluctuations attributable to baseflow from the subsurface. When storm runoff is excluded from the simulation, only the heat carried by direct groundwater discharge and by groundwater runoff controls stream temperature, yielding an excursion during warming at the model outlet of little more than 0.5 °C (Figure S3-4). It is worth noting, however, that there are periods of the year (possibly ecologically important) when, because storm runoff is largely absent, baseflow dominates streamflow and by extension its thermal regime,

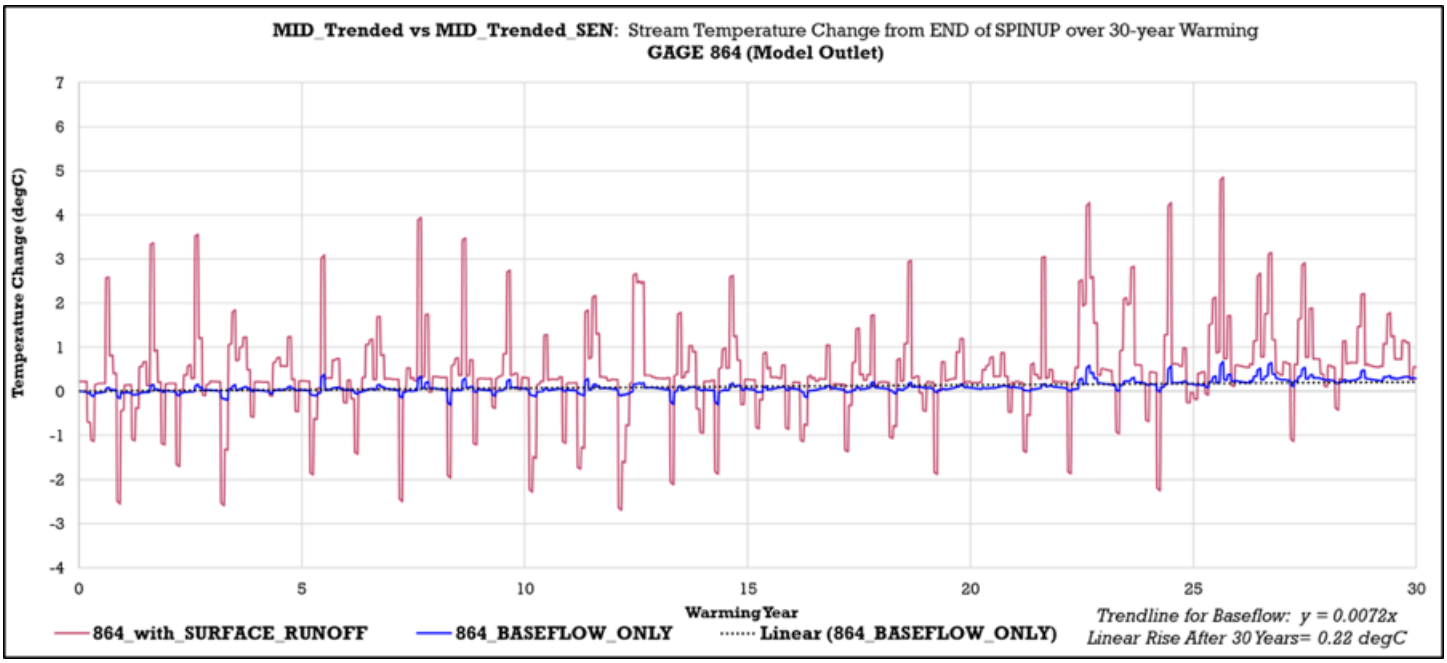

Figure S3-4. Comparison of temperature (°C) at model outlet gage in total streamflow to temperature in stream baseflow over warming period for MID_Trended simulation. Baseflow is the sum of direct groundwater discharge, groundwater discharge to riparian areas and rejected infiltration. Total streamflow is the sum of baseflow and storm runoff. Storm runoff dominates the total streamflow temperature signal; stream baseflow contributes most to temperature excursion in total streamflow during periods of low streamflow.

A second way to analyze the behavior of stream temperatures during warming is to quantify its upward trend, for example at the model outlet gage (864). Linear trendlines on the plots of the model outlet hydrograph in Figures S3-3b and S3-3d yield cumulative 30-year rises of 0.85 °C and 0.78 °C for the MID_TRENDED and HI_TRENDED simulations, respectively. Perhaps a more representative metric for the effect of warming arises corresponds to the difference between the average total streamflow temperature during the last 10 years of warming and the average temperature during the last year of spinup. For the MID_TRENDED simulation, the difference at the model outlet equals 0.48 °C for cool months (November-March) and 0.62 °C for warm months (April-October); the corresponding values for the HI_TRENDED simulation are slightly smaller: 0.44 °C and 0.61 °C. Accordingly, it is clear that for the conditions assumed in the synthetic model, the cumulative effect of climate forcing on total streamflow temperatures for a range of UZ thickness conditions is much weaker than the "natural" excursion in streamflow temperatures controlled by seasonal runoff. However, it also appears that the magnitude of the trend is comparable to the background excursion in baseflow temperatures (roughly 0.5 °C in both instances), and, therefore, potentially important for habitat viability in periods when baseflow is dominant or for organisms that live at the groundwater/surface-water interface at any time of year.

Simulation Results: Heat Fluxes and Heat Flows

Just as the dependent variable head is less suited to groundwater budget calculations than are model outputs in the form of volumetric flux and rates of flow, so in evaluating the circulation of heat it is often more instructive to represent model results in terms of heat flux or heat flow instead of temperature.

Because the energy propagation from the top of the UZ to the water table is represented through the UZF and UZT model packages as a one-dimensional process, it is straightforward to break down the simulated heat flux (Watts) into heat flow components moving downward through a unit horizontal area of one square meter (Watts/m^2). The components consist of convective, conductive and dispersive heat flows (any radiation components are neglected), which sum to the total rate of heat flow. Here heat flow components are more precisely defined drawing on the presentation in Morway et al., 2022.

It is possible on the basis of the governing transport equation to disaggregate the convective, conductive, and dispersive components of the heat energy flows. Using the volumetric fluxes, water contents, and calculated temperatures associated with a grid cell, the relative amounts of heat energy components transported through a grid cell may be calculated. As stated in Morway et al., 2022:

"The following equation relates the total change in the amount of energy stored in both the solid and aqueous phases within a control volume (i.e., grid cell) to the various components of the energy budget for that grid cell,

$$\dot{E}_{stor} = \dot{E}_{conv} + \dot{E}_{cond} + \dot{E}_{disp} + \dot{E}_{src/snk} + \dot{E}_{0^{th}} \quad (1)$$

where $\dot{E}_{stor}$ is the rate of energy change within a grid and is balanced by the following four components: $\dot{E}_{conv}$, the net convective energy that accompanies advective fluid flow into (and out of) a grid cell; $\dot{E}_{cond}$, the net bulk conductive energy entering a grid cell resulting from temperature gradients with neighboring cells within the matrix and fluid (assumed to be in thermal equilibrium); $\dot{E}_{disp}$, the net dispersive energy entering a grid cell slightly ahead or behind the main convective inflow owing to deviations in the actual velocity at the pore scale (Zheng and Wang 1999); $\dot{E}_{src/snk}$, the net energy directly imported or exported to or from a grid cell by way of an external fluid source or sink; and $\dot{E}_{0^{th}}$, the zeroth-order production or decay of heat."

In Morway et al., 2022, a section of the article is devoted to each of these energy rate terms. The method outlined there is applied in this study to explore ways to quantify the relative importance of the component terms for movement from the top of the UZ to the water table.

During the 30-year warming period, the mean convective, conductive, and dispersive heat flows to the water table for the MID_TRENDED simulation (averaged on a monthly basis across non-surface-water body cells) are 0.27, 0.013, and 0.000067 Watts/m^2, respectively. The corresponding outputs for the HI_TRENDED simulation are similar: 0.27, 0.011, and 0.000048 Watts/m^2. Because thermal gradients and, therefore, conductive and dispersive flows can be upward in the UZ whereas the convective flows are restricted by the kinematic wave method to the downward direction, a better measure of the relative strength of the three types of heat flow results from comparing the averages of their absolute values over the 360 monthly intervals. For the moderate relief simulation, the absolute value of the recharging conductive flows averages 11% of the convective flows, whereas the dispersive flows average 0.05%; for the high relief simulation, the corresponding ratios are 7% and 0.03%. Both model versions imply that convective flows dominate in recharge, a result that remains true under reasonable ranges for flow and transport parameters. In both versions, the total heat flow in recharge averages close to the convective value of 0.27 Watts/m^2, given that the conductive and dispersive values net close to zero. It is worth noting that thermal dispersion is a negligible heat flow component because we selected a small value of longitudinal dispersivity of 0.9 m (3 ft) relative to the lateral grid spacing of 91 m (300 ft), a choice consistent with the simplifying assumption that the synthetic

aquifer system is homogeneous. Explicit heterogeneity input at the grid scale or a larger dispersivity imposed at the subgrid scale would tend to cause more heat spreading in the subsurface, possibly lending increased importance to this heat flow component.

The influence of UZ thickness on total recharging heat flow and on heat flow components emerges when comparing trends over time (Figs. S3-6a, S3-6b). The MID_TRENDED convective results show appreciably

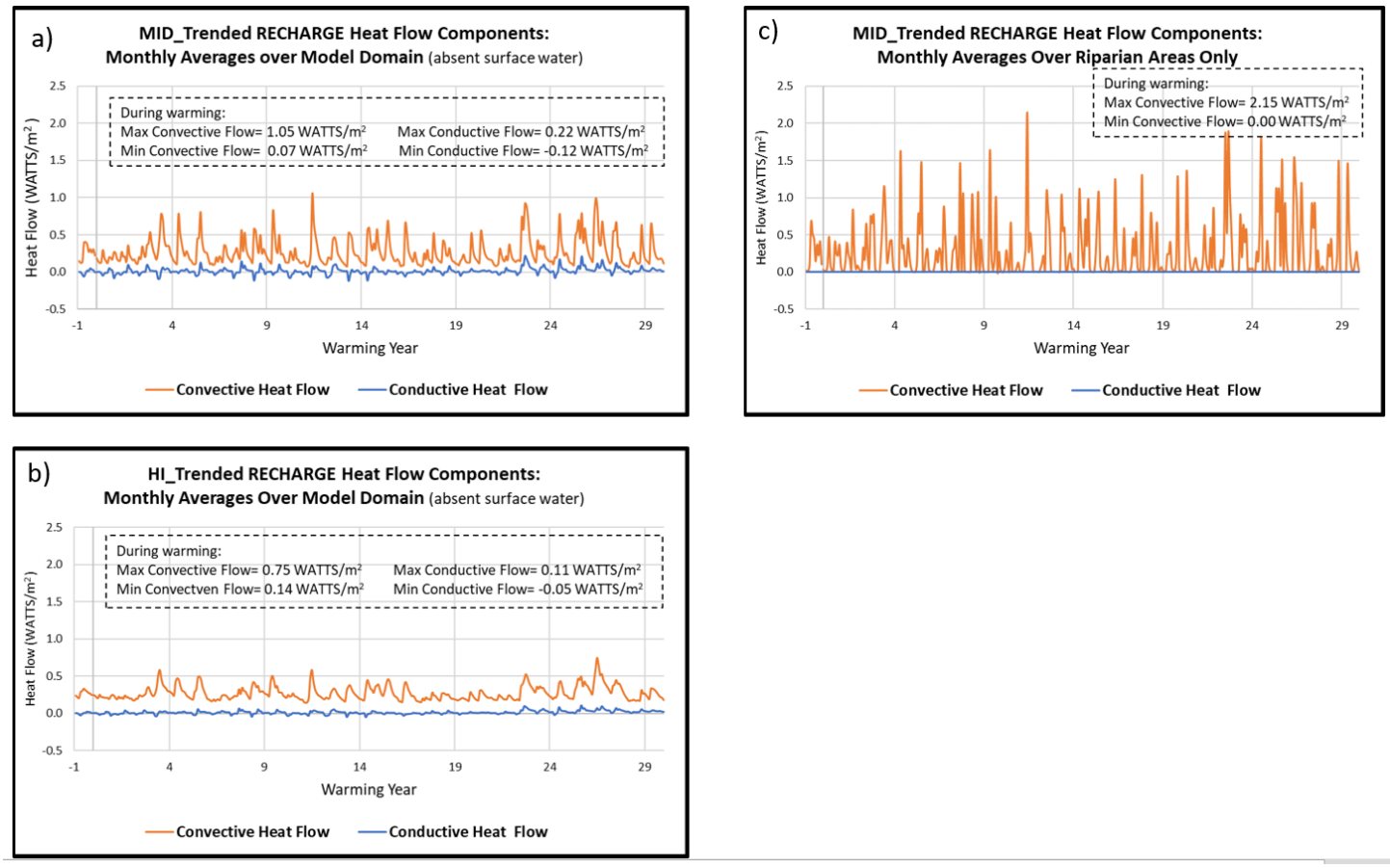

Figure S3-5. Recharge heat flow components (Watts/m2) averaged monthly over model domain for a) MID_TRENDED; b) HI_TRENDED, and c) MID_TRENDED for riparian areas only. Heat flow components are conduction and convection. Dispersive heat flux is negligible.

greater excursion (heat flows vary between 0.07 and 1.05 Watts/m²) than the HI_TRENDED case (between 0.14 and 0.75 Watts/m²); a similar relation holds true for the conductive flows. The UZ also influences results by way of its absence. In low-lying riparian areas where the water table is found in the upper three feet of the model (corresponding to model layer 1), the UZ loses its dampening capacity; the recharging convective heat flow equals the infiltrating heat inflow. In these areas, thermal conduction and dispersion are simulated as zero. For the moderate relief MID_TRENDED simulation, about 19% of the non-surface-water domain during the warming period is riparian (it ranges between 14% and 28% in response to head fluctuations). The maximum simulated rate of heat convection in recharge to the riparian areas averages about twice the maximum domain rate (compare Figure S3-5a and S3-5c), pointing to the potential importance of flat valleys in the efficient transfer of heat from the land surface to nearby streams draining the watershed. For the high relief simulation with steep-sided valleys, the average riparian extent is only about 3% of the non-surface-water domain, and under these conditions little heat is subject to rapid recharge and discharge through this pathway.

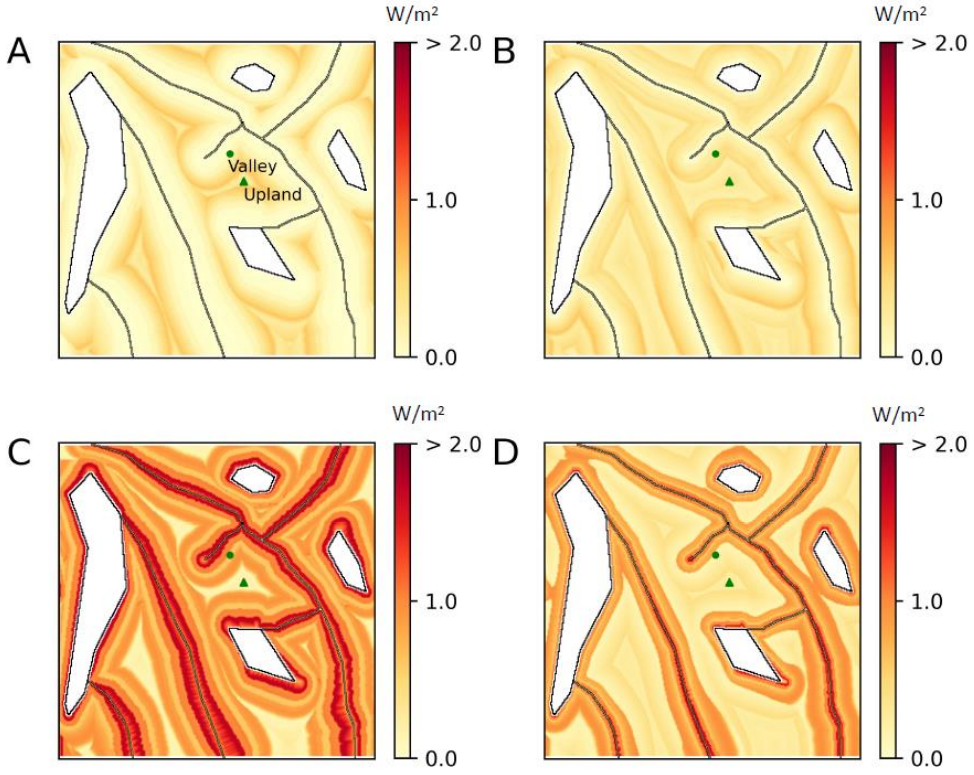

Figure S3-6. Maps of **total heat flow** (watts per meter squared) in recharge to water table for selected times during warming: A) MID_TRENDED, after 15.25 years of warming, month=March; B) HI_TRENDED, after 15.25 years of warming, month=March; C) MID_TRENDED, after 25.67 years of warming, month=August); D) HI_TRENDED, after 25.67 years of warming, month=August. Total heat flow is the sum of convective, conductive and dispersive flows.

The influence of the riparian areas also stands out when the total heat flow to the water table (convective + conductive + dispersive) is mapped for selected months during warming. Figure S3-6a shows the distribution of MID_TRENDED water-table results for a relatively cool month (March, 15.25 years into warming, moderate infiltration rate assigned 6.5 °C); Figure S3-6b does the same for the HI_TRENDED case. The rate of recharging heat flow for this interval is modest, less than 0.5 Watts/m². Close inspection suggests phase differences in the response for the MID and HI cases. Figure S3-6c shows the distribution of MID_TRENDED results for a relatively warm and wet month (August, 25.67 years into warming, high infiltration rate assigned 20.7 °C); Figure S3-6d corresponds to the HI_TRENDED results. The heat flow in recharge for this interval commonly exceeds 2.0 Watts/m², particularly in riparian areas along streams. These areas are much wider for the moderate-sloped case than the high-sloped one. Plots for both versions suggest a delay in the arrival of the thermal wave in the most upland areas of the watershed and ripple effects downslope. Recharging heat flow components also show spatial variation. The *conductive component* shows somewhat similar patterns but smaller magnitude (Figure S3-7). The conductive component depends on the direction of the thermal gradient in the UZ (and is negligible in saturated riparian areas), can be upward or downward (i.e., positive or negative), but always remains relatively smaller in absolute magnitude.

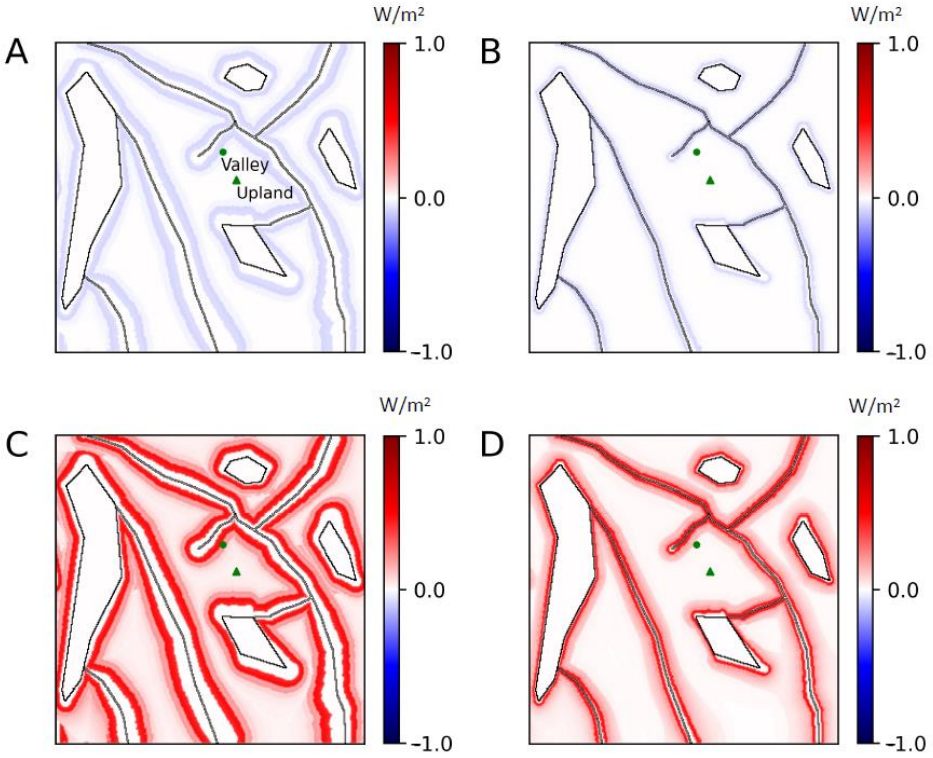

Figure S3-7. Maps of **conductive heat flow** in watts per meter squared in recharge to water table for selected times during warming. a) MID_TRENDED, after 15.25 years of warming (month=March); b) HI_TRENDED, after 15.25 years of warming (month=March); c) MID_TRENDED, after 25.67 years of warming (month=August) and d) HI_TRENDED, after 25.67 years of warming (month=August).

Simulation Results: Lags and Dampening of Heat Signal

There are three main interfaces at the beginning or end of watershed pathways where the three heat flux components in principle could be calculated: across the top of the UZ (infiltration), across the water table (recharge) and across a streambed or lake bed (baseflow). They are discussed in turn:

- In this study the thermal infiltration is equated with the heat movement downward from the bottom of the root zone which occurs after processes of runoff and evapotranspiration have rerouted some of the water and heat along the land surface or to the atmosphere. This net heat flow is approximated as a purely downward convective process into the top of the UZ. For the purposes of this study, the combined effect of heat conduction and dispersion at the root zone/UZ interface, either upward or downward, is considered to be negligible in comparison to the surface and root zone processes that determine the rate of infiltrating heat flux.
- Analysis of the relative weight of simulated heat transport components out of the UZ show that for humid temperate conditions of the synthetic model, the convective heat flow dominates the conductive and dispersive flow at the water-table interface. This relation is true over time at the scale of individual model cells (Figure S3-10) and when averaged over the entire model domain (Figure S3-5). For the MID_TRENDED simulation, the absolute value of the conductive heat flows at the water table average about 11% of the convective heat flow, whereas the dispersive heat flow is only 0.05% of the convective heat flow. For the HI_TRENDED simulation, the corresponding ratios are 7% and 0.03%. It is worth noting that thermal dispersion is a negligible heat flow component owing to the relatively small longitudinal dispersivity specified (0.9 m) relative to the lateral grid spacing [91 m (300 ft)], a choice consistent with a homogeneous synthetic aquifer. These findings suggest that there is in general only minor

loss of accuracy if the heat flow across the interface at the top of the groundwater system is approximated by considering the convective heat flux alone.

- The temperature gradient across the streambed between the stream water in the channel and the ambient groundwater could be incorporated in equations that yield convective and dispersive components of heat flow. Thermal conduction would occur whether the temperature gradient is in the same direction as baseflow or in the opposite direction away from the stream; dispersion would occur only when the gradient is in the same direction as the flow through the streambed. However, the MT3D-USGS code neglects these theoretical components of heat flux and only calculates the convective component either as a function of groundwater temperature in the presence of baseflow or as a function of streamflow temperatures in the presence of stream loss.

Given that heat flux across the major watershed interfaces is either imposed as convective flux, approximated by convective flux, or only calculated as convective flux, it is convenient in the pathway analysis of thermal lagging and dampening presented below to define heat movement in relation strictly to the magnitude and direction of water flow, neglecting the conductive and dispersive fluxes.

The convective movement of heat from the top of the UZ downgradient to the surface-water network is a form of energy propagation. The amount of heat energy that passes is a function of the rate of water movement and the temperature of the water. A convenient unit for the accumulated heat flux is Watts (joules/sec). A convenient unit for the rate of heat flux, that is the heat flow, is Watts/m^2, equivalent to the heat flux divided by an appropriate area. Table S3-1 contains the equations for convective heat flux (quantified in terms of water flux, water temperature, the specific heat of water, and its density). Heat fluxes along the successive pathways pictured in Feinstein et al. (2022) Figure 1 are quantified for the contributing basins upstream of gage locations shown in Supplemental Information Appendix Figure S2-3. The surface and subsurface heat fluxes are normalized by dividing them either by a unit cross-sectional area perpendicular to the flow direction or by contributing basin areas to generate the average heat flows for the basin. The contributing basins are nested: the basin associated with Gage 864, for example, includes the entire stream drainage for the eastern side of the model.

Table S3-1. Convective Heat Flux and Heat Flow: Units and Conversions.

Energy Flux = Heat Flux [Joules/second, equivalent to Watts] = Water Volumetric Flux x Water Temperature x Specific Heat of Water x Water Density	
Specific heat of water =	4183 joules/(kg-^{o}C)
Density of water =	28.32 kg/ft^3 = 1000 kg/m^3
Heat Flux can refer to successive thermal pathways:	
• Infiltration to top of UZ • Surface runoff to surface water • Recharge to water table • Groundwater runoff to surface water originating as rejected infiltration • Groundwater runoff to surface water originating as discharge to riparian land surface • Groundwater discharge directly to surface water • Accumulated baseflow from upstream in stream channel • Accumulated total streamflow from upstream in stream channel	
Note: Energy Flow = **Rate of Heat Flow** [Watts/m^2] = *Heat Flux / Area* *Area [m^2]* can refer to a unit surface perpendicular to the direction of heat flux or to a normalizing basin area applied to each heat pathway	

Energy Flux = **Heat Flux** [Joules/second, equivalent to Watts] =
Water Volumetric Flux x Water Temperature x Specific Heat of Water x Water Density

Specific Heat of Water = 4183 joules/(kg-degC)
Density of Water = 28.32 kg/ft^3 = 1000 kg/m^3

Heat Flux can refer to successive thermal pathways:
- Infiltration to top of UZ
- Surface runoff to surface water
- Recharge to water table
- Groundwater runoff to surface water originating as rejected infiltration
- Groundwater runoff to surface water originating as discharge to riparian land surface
- Groundwater discharge directly to surface water
- Accumulated baseflow from upstream in stream channel
- Accumulated total streamflow from upstream in stream channel

****

Energy Flow = **Rate of Heat Flow** [Watts/m^2] = *Heat Flux / Area*

Area [m^2] can refer to a unit surface perpendicular to the direction of heat flux or to a normalizing basin area applied to each heat pathway

The convective heat flux accumulated over contributing basins for different pathways and averaged over different periods is represented in Figure S3-5 for the MID_TRENDED and HI_TRENDED simulations. Heat flux diminishes in strength from infiltration to recharge to discharge pathways as a consequence of heat storage (which causes rising temperatures). Direct heat flux discharge to streams is greater for the HI than the MID simulation partly because, given the configuration of land surface, there is less riparian area in the former to receive groundwater heat discharge and also less occasion for rejected infiltration. For both model versions, the incoming heat flux averaged over the last 10 years of warming is appreciably greater than the amount averaged over the last year of spinup. However, the difference between spinup and warming conditions becomes much smaller in the outgoing heat flux owing to implicit heat storage effects.

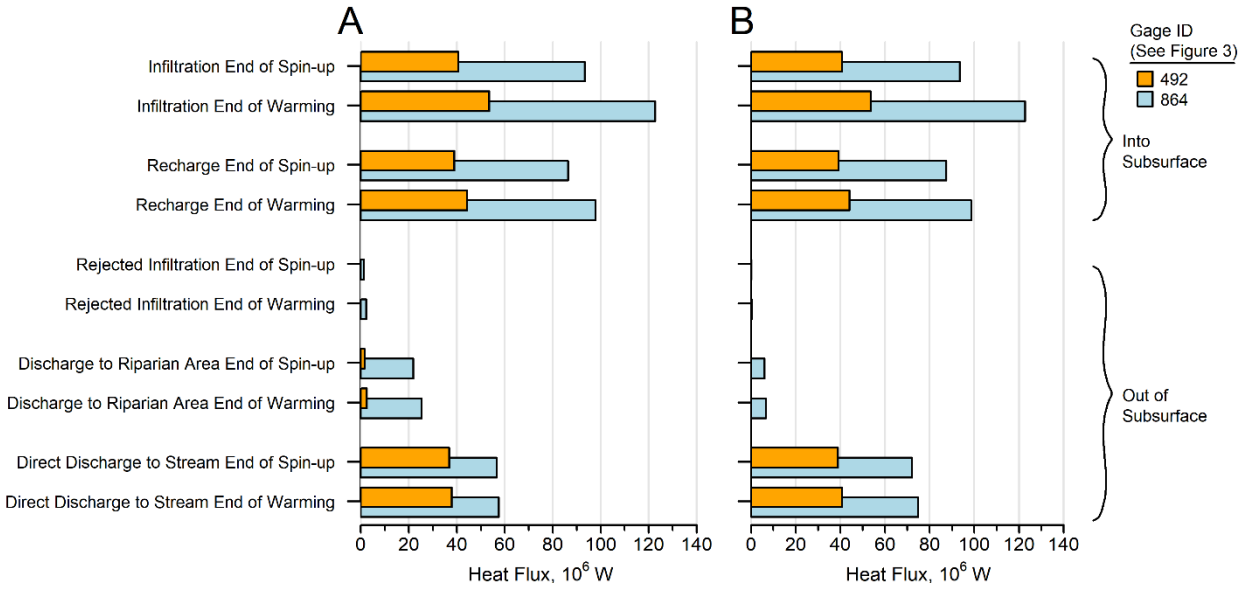

Figure S3-8. Convective heat flux (Watts) accumulated over contributing basins upgradient of gage locations for the MID_TRENDED (a) and HI_TRENDED (b) models. Infiltration flux is compared to flux transmitted by down-system pathways. Convective flux for each pathway corresponds to average for last year of spinup and to average for average of last 10 years of warming.

Quantification of amplitude and phase relations between heat inflows and down-system heat flows and temperatures is yet another way to characterize watershed heat transport. The **lag analysis** consists of a series of impulse/response calculations at the scale of the nested contributing basins. The impulse is the heat flow (equivalent to heat flux normalized by contributing basin areas) in infiltration (or, when noted, infiltration plus storm runoff). The response corresponds to one of the following six pathways:

- heat flow in recharge to the water table above gage;
- heat flow in direct groundwater discharge to streams above gage;
- heat flow in baseflow to streams above gage (equivalent to total discharge, that is, the sum of rejected infiltration + groundwater discharge to riparian zone + direct groundwater discharge);
- heat flow in total streamflow at gage location (the heat impulse equals the sum of infiltration and storm runoff; the heat response equals the sum of baseflow and storm runoff in the stream channel);
- flux-weighted temperature in direct groundwater discharge to streams above gage;
- temperature in total streamflow at gage location (the heat impulse equals sum of infiltration and storm runoff; the heat response equals the temperature of combined baseflow and storm runoff in streamflow)

Correlation coefficients computed at different monthly offsets (from 0 months to 6 or 12 months) between the (causal) impulse and (caused) response are equated with the size of the lag effect. For example, strong correlation coefficients for two- and three-month offsets, and weak coefficients for the other offsets, implies that the dominant lag interval is two to three months in duration. Coefficient values above 0.3 are taken to indicate a strong correlation. The **dampening analysis** is more straightforward—it is expressed by the ratio of the average heat flow (or temperature in case of streamflow) for the last 10 years of warming to the average heat flow value for the last year of spinup. As in the case of the lag analysis, the ratio is calculated for the successive pathways across each of the nested gage contributing basins.

In tracking heat flows, an effort has been made to quantify explicitly the important pathways; however, some sink/sources of heat have not been explicitly quantified. The lake simulated in the synthetic model functions as a small sink/source of heat—its effect

on the thermal load of downgradient stream reaches is not explicitly analyzed. More importantly, storage uptake in the UZ and saturated system influences the model results by delaying the movement of heat; this effect is implicit in the lag and dampening analysis presented below

A good way to visualize lags and dampening is to start with heat flow from the top of the UZ to the water table. Delays in timing and muting of the size of the recharging heat flow at any location is, again, strongly influenced

- by the thickness of the UZ. The plots in Figure S3-9, containing results for the last 10 years of warming, show distinct behavior for the UPLAND (relatively thick UZ) and VALLEY (relatively thin UZ) locations, further
- accentuated by the contrast between the moderate relief MID_TRENDED simulation and the high relief HI_TRENDED simulation. The phase and amplitude shifts associated with distinct UZ thicknesses are evident when the heat flow arriving at the water table (red or blue solid lines) is compared with the heat inflow at the top of the UZ (light blue bars). For the UPLAND location associated with the HI land surface (water table depth around 32 m or 106 ft), the total heat flow recharging the groundwater is quite stable, and, consequently, fluctuations due to large month-to-month variations in infiltration forcing are largely smoothed. For the other cases where water table depths range between 3m and 14m (11 ft and 46 ft), the heat flow breakthrough at the water table remains responsive to the energy frequencies imposed by infiltration.

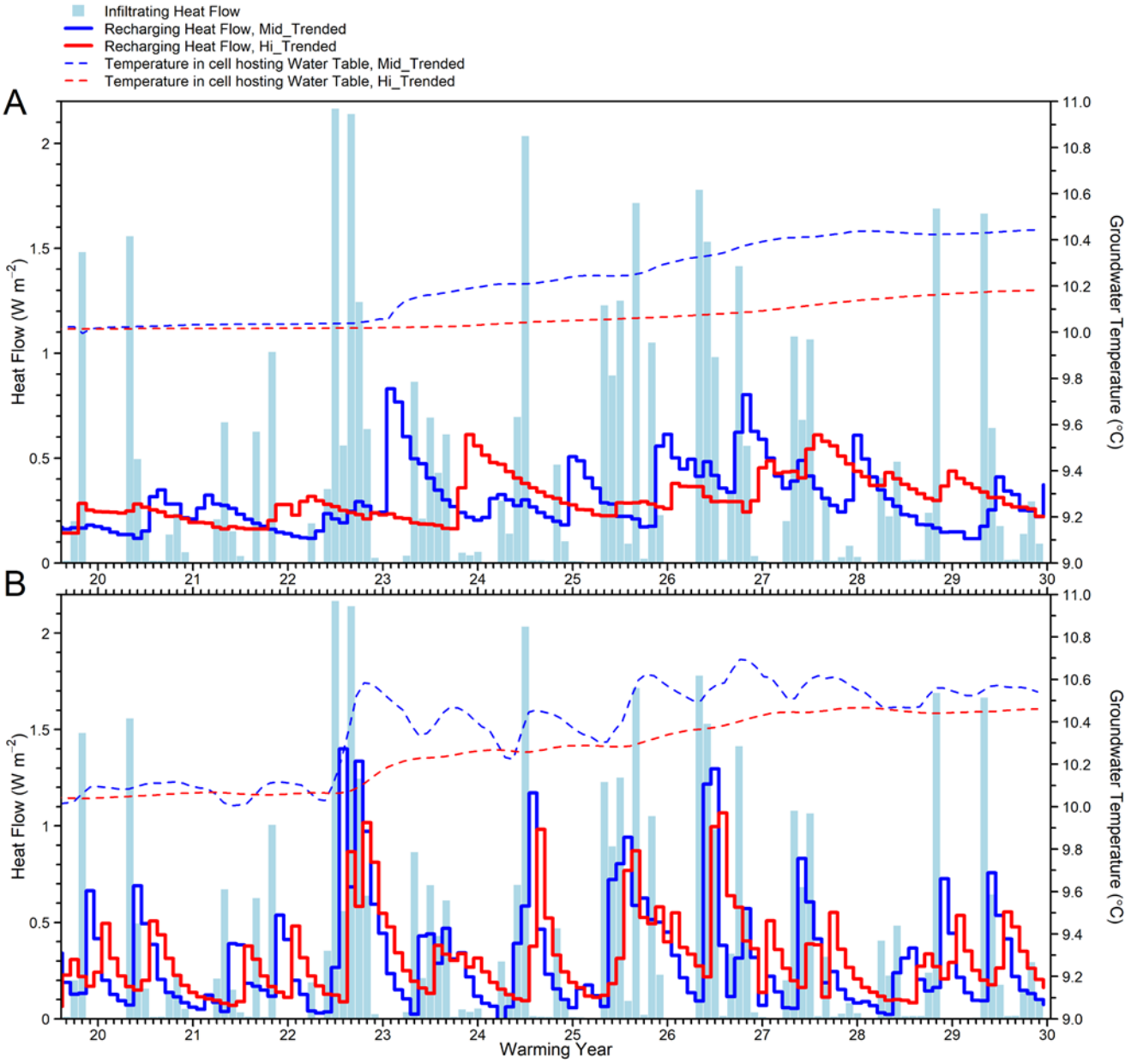

Figure S3-9. Convective **h**eat flow (Watts/m²) and temperature (ºC) in recharge to water table at UPLAND (A) and VALLEY (B) locations for MID_TRENDED and HI_TRENDED simulations for last 10 years of warming period showing lags and dampening between infiltrating heat flow and recharging heat flow.

The temperature responses at the water table at the two locations (the dashed curves in Figure S3-9) also reflect the inertial force of the saturated water volume in the model cells. The temperature follows either a smooth trendline or, for the most shallow water-table case, a damped sine wave. As already noted, the rate of recharging heat flow is determined chiefly by convection; the conduction contribution is small, although sometimes oriented upward (see Figure S3-10 showing conductive and total heat flow for the VALLEY location over the last 10 years of warming).

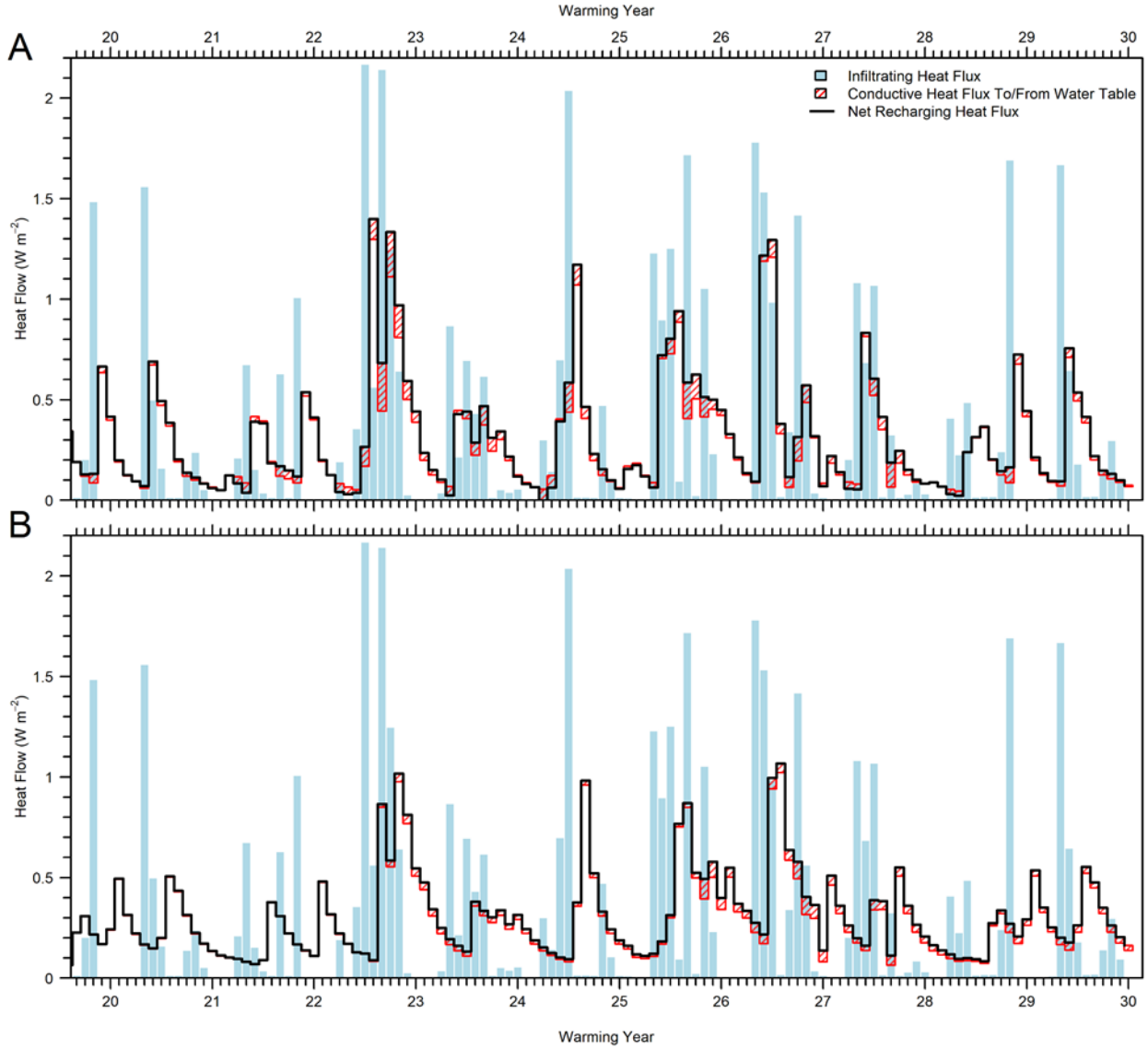

Figure S3-10. Conductive component and total heat flow (Watts/m^2) in recharge to water table at VALLEY location for (A) MID_TRENDED and (B) HI_TRENDED simulations for last 10 years of warming period. The dispersive component is negligible.

The hydrographs in Figure S3-9 can be subjected to a formal lag analysis by quantifying correlation coefficients between infiltrating heat flow and recharging heat flow at different monthly offsets—see Table S3-2. At the UPLAND location, the impulse/response delay for the moderately-sloped model is quite long, on the order of 7-8 months. For the highly-sloped model there is little relation between the impulse and response—because of the UZ exceeding 30 m (100 ft), the recharging heat flow is largely steady whatever the thermal fluctuations near the land surface. The story is different at the VALLEY location where the water table is shallower. The MID_TRENDED simulation shows strong correlation peaking at a one-month lag; the HI_TRENDED simulation shows a slightly less strong correlation peaking at a two-month lag.

Table S3-2. Lag correlation of heat inflow with convective heat flow (Watts/m2) to water table at UPLAND and VALLEY locations for MID_TRENDED and HI_TRENDED simulations over warming period. Heat inflow is spatially uniform over model domain. Correlation coefficients greater than 0.3 are highlighted in yellow. Maximum value for each model version is in **bold** face.

Month lag over all warming	MID_Trended Upland	HI_TRENDED Upland	MID_TRENDED Valley	HI_TRENDED Valley
-1	-0.032	-0.073	-0.006	-0.084
0	-0.022	-0.056	0.203	-0.023
1	0.024	-0.067	**0.791**	0.141
2	-0.019	-0.050	0.437	**0.560**
3	-0.021	-0.006	0.170	0.536
4	-0.004	0.042	-0.023	0.333
5	0.130	0.039		0.132
6	0.320	0.053		-0.068
7	**0.428**	**0.089**		
8	0.383	0.065		
9	0.247	0.035		
10	0.116	0.004		
11	0.051			
12	0.029			
Dominant lag period	7-8 months	None	1-2 months	2-4 months
Dominant month lag	7	None	1	2

The model produces a wealth of output related to lags and dampening for not only the recharge pathway but also for down-system subsurface and surface pathways. It is convenient to integrate these results at the contributing basin scale by summing up heat fluxes and dividing them by the appropriate basin area. In Figure S3-11, a-f, heat flow and temperature responses for six pathways is graphed for a small headwater basin and for the large outlet basin. Table S3-3 distills the lag findings in terms of the offset and strength of correlation coefficients for each pathway. Integrated at the basin scale, the lags are less pronounced than for recharge at the individual UPLAND and VALLEY locations and tend to decrease down-system. Peak heat flow lags are only modestly longer for the high-sloped case than for the moderately-sloped. Specifically, direct groundwater discharge to streams at the model outlet gage displays a longer lag time than does recharge for both versions, but the delay is modest, on the order of an additional month.

A

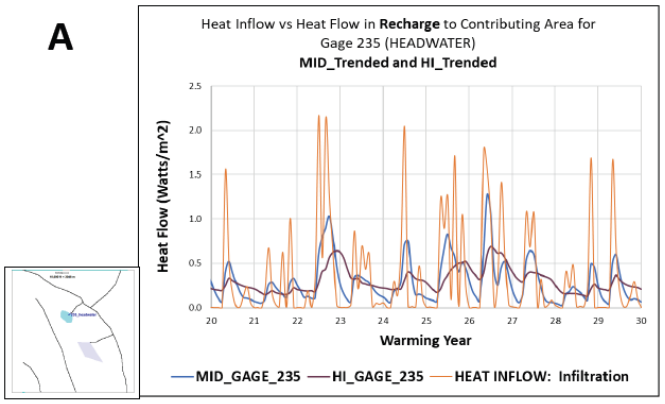

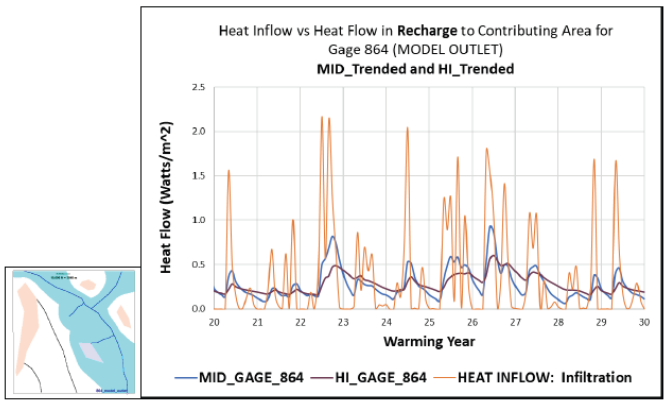

MID_Trended

LAGGED CORRELATION BETWEEN HEAT INFLOW and HEAT FLOW in RECHARGE to WATER TABLE

Correlations stronger than 0.3 are highlighted; maximum gage correlation in boldface.

Monthly Lag	Gage 235	Gage 285	Gage 492	Gage 692	Gage 864
-1	0.089	0.037	0.061	0.062	0.068
0	0.652	0.501	0.588	0.594	0.620
1	**0.704**	**0.629**	**0.677**	**0.671**	**0.667**
2	0.347	0.450	0.422	0.424	0.411
3	0.040	0.286	0.202	0.203	0.182
4	-0.140	0.136	0.030	0.029	0.010
5	-0.219	0.014	-0.084	-0.087	-0.101
6	-0.114	0.006	-0.051	-0.053	-0.055
AVERAGE 20-30 years	**0.291**	**0.300**	**0.292**	**0.280**	**0.281**
Ratio to Last Year of Spinup	**1.128**	**1.141**	**1.135**	**1.134**	**1.133**

HI_Trended

LAGGED CORRELATION BETWEEN HEAT INFLOW and HEAT FLOW in RECHARGE to WATER TABLE

Correlations stronger than 0.3 are highlighted; maximum gage correlation in boldface.

Monthly Lag	Gage 235	Gage 285	Gage 492	Gage 692	Gage 864
-1	-0.018	-0.004	-0.005	0.002	0.008
0	0.241	0.173	0.220	0.259	0.297
1	**0.481**	**0.421**	**0.524**	**0.514**	**0.515**
2	0.424	0.348	0.415	0.405	0.400
3	0.369	0.285	0.325	0.310	0.299
4	0.292	0.201	0.210	0.201	0.192
5	0.212	0.139	0.125	0.121	0.115
6	0.160	0.120	0.093	0.102	0.107
AVERAGE 21-30 years	**0.303**	**0.297**	**0.291**	**0.281**	**0.283**
Ratio to Last Year of Spinup	**1.144**	**1.125**	**1.126**	**1.127**	**1.127**

Figure S3.-11 a: Convective HEAT FLOW response (Watts/m^2) along RECHARGE pathway for MID_TRENDED and HI_TRENDED simulations. Graphs compare impulse heat flow in INFILTRATION to response heat flow in the pathway during the last 10 years of warming for contributing basins corresponding to headwater gage (235) and model outlet gage (864). Heat Flow = Heat Flux over basin normalized by basin area. Top table shows correlation coefficients between infiltration and recharge for five gage locations along stream network at different monthly time offsets (used in lag analysis). Bottom table shows change in recharge heat flow between average for last year of spinup and last 10 years of warming for five gage locations along stream network (used in dampening analysis). Correlation coefficients greater than 0.3 are highlighted in yellow. Maximum value for each model version is in **bold** face; orange color demarcates pathway of interest.

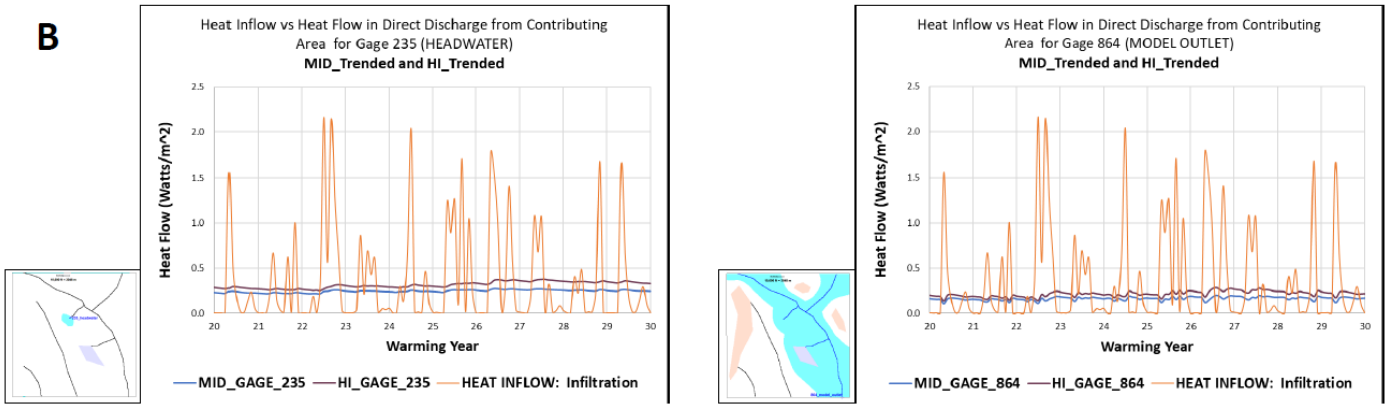

MID_Trended

LAGGED CORRELATION BETWEEN HEAT INFLOW and HEAT FLOW in DIRECT GROUNDWATER DISCHARGE

Correlations stronger than 0.3 are highlighted; maximum gage correlation in boldface.

Monthly Lag	Gage 235	Gage 285	Gage 492	Gage 692	Gage 864
-1	-0.018	-0.062	-0.106	-0.146	-0.186
0	0.400	0.169	-0.088	-0.314	-0.661
1	**0.441**	**0.582**	**0.560**	**0.489**	0.291
2	0.307	0.428	0.432	0.415	0.308
3	0.170	0.296	0.346	0.377	**0.363**
4	0.068	0.133	0.175	0.208	0.232
5	0.012	0.038	0.075	0.105	0.143
6	0.069	0.014	-0.006	-0.027	-0.055
AVERAGE 20-30 years	**0.247**	**0.185**	**0.250**	**0.179**	**0.165**
Ratio to Last Year of Spinup	**1.014**	**1.035**	**1.029**	**1.024**	**1.016**

HI_Trended

LAGGED CORRELATION BETWEEN HEAT INFLOW and HEAT FLOW in DIRECT GROUNDWATER DISCHARGE

Correlations stronger than 0.3 are highlighted; maximum gage correlation in boldface.

Monthly Lag	Gage 235	Gage 285	Gage 492	Gage 692	Gage 864
-1	-0.076	-0.106	-0.118	-0.130	-0.148
0	0.101	-0.116	-0.232	-0.297	-0.389
1	**0.293**	**0.452**	**0.448**	**0.426**	**0.380**
2	0.244	0.369	0.374	0.376	0.360
3	0.182	0.316	0.339	0.352	0.359
4	0.103	0.178	0.197	0.210	0.223
5	0.052	0.093	0.110	0.119	0.132
6	0.044	0.006	-0.006	-0.013	-0.018
AVERAGE 21-30 years	**0.316**	**0.203**	**0.269**	**0.198**	**0.215**
Ratio to Last Year of Spinup	**1.029**	**1.042**	**1.048**	**1.050**	**1.037**

Figure S3.-11 b. (cont): Convective HEAT FLOW response (Watts/m²) along DIRECT GROUNDWATER DISCHARGE pathway for MID_TRENDED and HI_TRENDED simulations. Graphs compare impulse heat flow in INFILTRATION to response heat flow in the pathway during the last 10 years of warming for contributing basins corresponding to headwater gage (235) and model outlet gage (864). Heat Flow = Heat Flux over basin normalized by basin area. Top table shows correlation coefficients between infiltration and direct groundwater discharge for five gage locations along stream network at different monthly time offsets (used in lag analysis). Bottom table shows change in direct groundwater discharge heat flow between average for last year of spinup and last 10 years of warming for five gage locations along stream network (used in dampening analysis). Correlation coefficients greater than 0.3 are highlighted in yellow. Maximum value for each model version is in **bold** face; orange color demarcates pathway of interest.

.

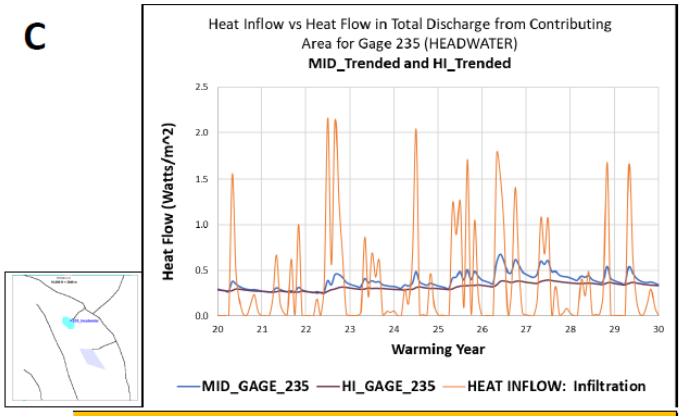

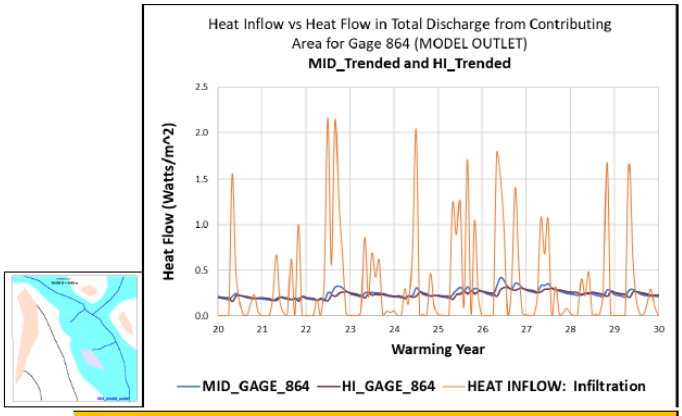

MID_Trended

LAGGED CORRELATION BETWEEN HEAT INFLOW and HEAT FLOW in BASEFLOW DISCHARGE

Correlations stronger than 0.3 are highlighted; maximum gage correlation in boldface.

Monthly Lag	Gage 235	Gage 285	Gage 492	Gage 692	Gage 864
-1	0.046	-0.010	-0.027	0.004	0.028
0	**0.657**	0.415	0.306	0.472	**0.582**
1	0.355	**0.522**	**0.572**	**0.553**	0.531
2	0.222	0.359	0.399	0.379	0.350
3	0.052	0.196	0.241	0.194	0.150
4	0.008	0.080	0.105	0.073	0.045
5	-0.033	0.005	0.019	-0.010	-0.031
6	0.070	0.035	0.015	0.020	0.024
AVERAGE 20-30 years	**0.383**	**0.210**	**0.269**	**0.230**	**0.245**
Ratio to Last Year of Spinup	**1.075**	**1.060**	**1.060**	**1.068**	**1.068**

HI_Trended

LAGGED CORRELATION BETWEEN HEAT INFLOW and HEAT FLOW in BASEFLOW DISCHARGE

Correlations stronger than 0.3 are highlighted; maximum gage correlation in boldface.

Monthly Lag	Gage 235	Gage 285	Gage 492	Gage 692	Gage 864
-1	-0.070	-0.105	-0.118	-0.111	-0.118
0	0.133	-0.104	-0.230	-0.156	-0.184
1	**0.288**	**0.449**	**0.448**	**0.464**	**0.445**
2	0.236	0.366	0.374	0.394	0.389
3	0.168	0.311	0.338	0.340	0.341
4	0.095	0.175	0.197	0.195	0.201
5	0.047	0.092	0.109	0.100	0.105
6	0.046	0.007	-0.006	-0.006	-0.008
AVERAGE 21-30 years	**0.320**	**0.203**	**0.269**	**0.221**	**0.235**
Ratio to Last Year of Spinup	**1.038**	**1.044**	**1.049**	**1.051**	**1.044**

Figure S3.-11 c. (cont): Convective HEAT FLOW response (Watts/m^2) along BASEFLOW (= TOTAL DISCHARGE) pathway for MID_TRENDED and HI_TRENDED simulations. Graphs compare impulse heat flow in INFILTRATION to response heat flow in the pathway during the last 10 years of warming for contributing basins corresponding to headwater gage (235) and model outlet gage (864). Heat Flow = Heat Flux over basin normalized by basin area. Top table shows correlation coefficients between infiltration and baseflow for five gage locations along stream network at different monthly time offsets (used in lag analysis). Bottom table shows change in baseflow heat flow between average for last year of spinup and last 10 years of warming for five gage locations along stream network (used in dampening analysis). Correlation coefficients greater than 0.3 are highlighted in yellow. Maximum value for each model version is in **bold** face; orange color demarcates pathway of interest.

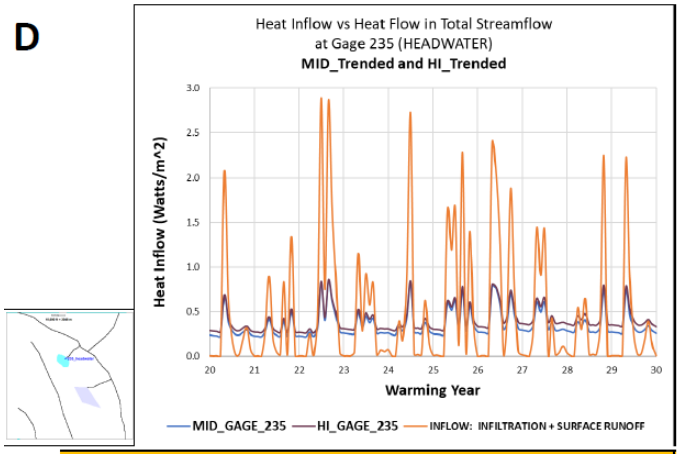

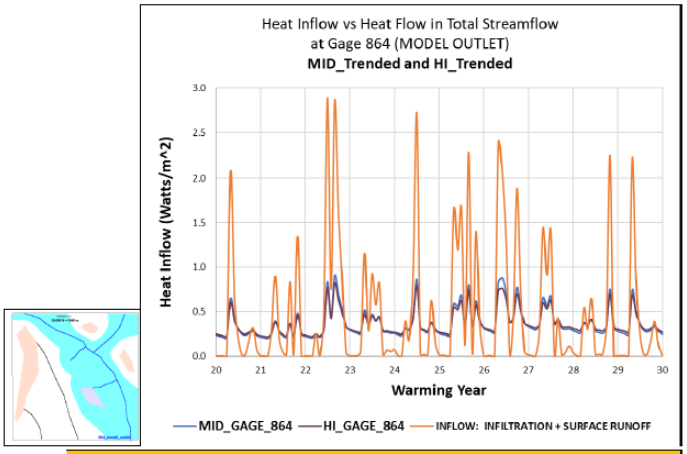

MID_Trended

LAGGED CORRELATION BETWEEN HEAT INFLOW and HEAT FLOW in TOTAL STREAMFLOW

Correlations stronger than 0.3 are highlighted; maximum gage correlation in boldface.

Monthly Lag	Gage 235	Gage 285	Gage 492	Gage 692	Gage 864
-1	0.137	0.133	0.128	0.120	0.125
0	**0.992**	**0.987**	**0.977**	**0.953**	**0.964**
1	0.198	0.226	0.263	0.319	0.297
2	0.092	0.114	0.140	0.185	0.166
3	-0.113	-0.095	-0.075	-0.040	-0.056
4	-0.077	-0.068	-0.059	-0.049	-0.056
5	-0.128	-0.126	-0.122	-0.117	-0.120
6	0.017	0.013	0.009	0.011	0.012
AVERAGE 20-30 years	**0.360**	**0.296**	**0.383**	**0.364**	**0.374**
Ratio to Last Year of Spinup	**1.087**	**1.127**	**1.121**	**1.129**	**1.127**

HI_Trended

LAGGED CORRELATION BETWEEN HEAT INFLOW and HEAT FLOW in TOTAL STREAMFLOW

Correlations stronger than 0.3 are highlighted; maximum gage correlation in boldface.

Monthly Lag	Gage 235	Gage 285	Gage 492	Gage 692	Gage 864
-1	0.127	0.133	0.126	0.118	0.120
0	**0.981**	**0.989**	**0.978**	**0.954**	**0.962**
1	0.199	0.210	0.249	0.308	0.289
2	0.101	0.107	0.138	0.185	0.172
3	-0.102	-0.099	-0.073	-0.037	-0.047
4	-0.068	-0.066	-0.051	-0.039	-0.042
5	-0.124	-0.126	-0.120	-0.113	-0.115
6	0.015	0.009	0.006	0.007	0.007
AVERAGE 21-30 years	**0.409**	**0.293**	**0.382**	**0.363**	**0.371**
Ratio to Last Year of Spinup	**1.080**	**1.116**	**1.111**	**1.117**	**1.111**

Figure S3-11. d. (cont): Convective HEAT FLOW response (Watts/m^2) along TOTAL STREAMFLOW pathway (including storm runoff) for MID_TRENDED and HI_TRENDED simulations. Graphs compare impulse heat flow in INFILTRATION to response heat flow in the pathway during the last 10 years of warming for contributing basins corresponding to headwater gage (235) and model outlet gage (864). Heat Flow = Heat Flux over basin normalized by basin area. Top table shows correlation coefficients between infiltration and total streamflow for five gage locations along stream network at different monthly time offsets (used in lag analysis). Bottom table shows change in total streamflow heat flow between average for last year of spinup and last 10 years of warming for five gage locations along stream network (used in dampening analysis). Correlation coefficients greater than 0.3 are highlighted in yellow. Maximum value for each model version is in **bold** face; orange color demarcates pathway of interest.

E

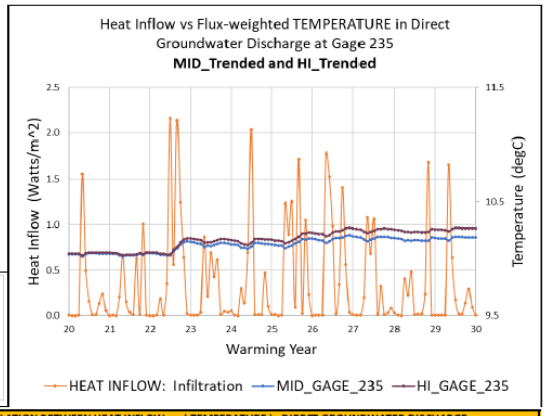

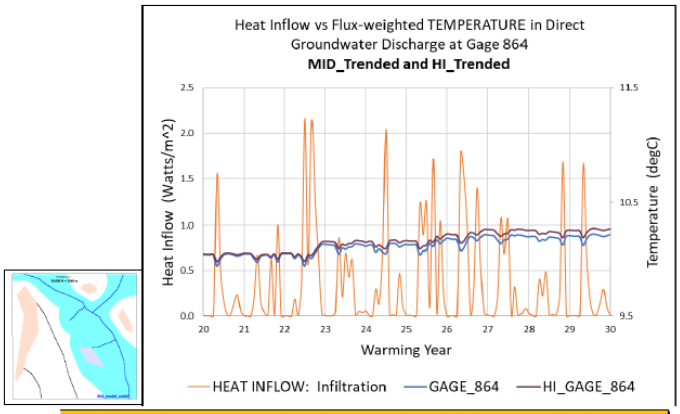

MID_Trended

LAGGED CORRELATION BETWEEN HEAT INFLOW and TEMPERATURE in DIRECT GROUNDWATER DISCHARGE

Correlations stronger than 0.3 are highlighted; maximum gage correlation in boldface.

Monthly Lag	Gage 235	Gage 285	Gage 492	Gage 692	Gage 864
-1	-0.014	-0.029	-0.055	-0.059	-0.054
0	-0.032	-0.160	-0.278	-0.301	-0.297
1	0.114	0.109	0.073	0.033	0.037
2	0.158	0.166	0.171	0.154	0.152
3	0.188	**0.204**	**0.228**	**0.227**	**0.220**
4	**0.199**	0.193	0.213	0.220	0.216
5	0.199	0.185	0.196	0.202	0.199
6	0.162	0.125	0.110	0.112	0.111
AVERAGE 20-30 years	10.126	10.153	10.124	10.125	10.117
Ratio to Last Year of Spinup	1.013	1.016	1.015	1.014	1.013

HI_Trended

LAGGED CORRELATION BETWEEN HEAT INFLOW and TEMPERATURE in DIRECT GROUNDWATER DISCHARGE

Correlations stronger than 0.3 are highlighted; maximum gage correlation in boldface.

Monthly Lag	Gage 235	Gage 285	Gage 492	Gage 692	Gage 864
-1	0.001	-0.015	-0.033	-0.035	-0.029
0	-0.003	-0.117	-0.206	-0.217	-0.172
1	0.090	0.094	0.073	0.042	0.040
2	0.130	0.140	0.149	0.136	0.123
3	0.158	**0.173**	**0.193**	**0.192**	0.175
4	0.175	0.170	0.185	0.191	**0.181**
5	**0.182**	0.169	0.177	0.183	0.179
6	0.160	0.129	0.116	0.119	0.129
AVERAGE 21-30 years	10.168	10.165	10.143	10.149	10.153
Ratio to Last Year of Spinup	1.017	1.017	1.016	1.016	1.013

Figure S3.-11 e. (cont.): TEMPERATURE response (°C) along DIRECT GROUNDWATER DISCHARGE pathway for MID_TRENDED and HI_TRENDED simulations. Graphs compare impulse heat flow in INFILTRATION to response TEMPERATURE in the pathway during the last 10 years of warming for contributing basins corresponding to headwater gage (235) and model outlet gage (864). Top table shows correlation coefficients between infiltration and direct groundwater discharge for five gage locations along stream network at different monthly time offsets (used in lag analysis). Bottom table shows change in direct groundwater discharge temperature between average for last year of spinup and last 10 years of warming for five gage locations along stream network (used in dampening analysis). Correlation coefficients greater than 0.3 are highlighted in yellow. Maximum value for each model version is in **bold** face; orange color demarcates pathway of interest.

F

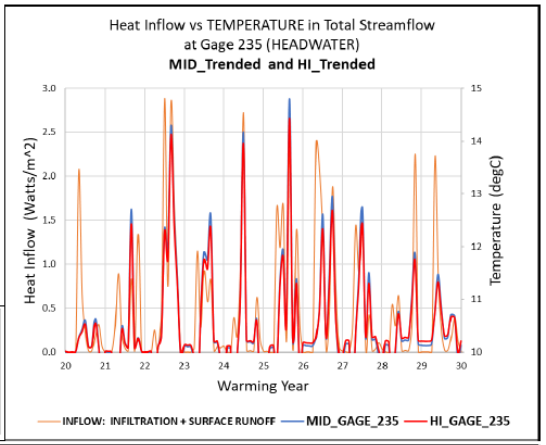

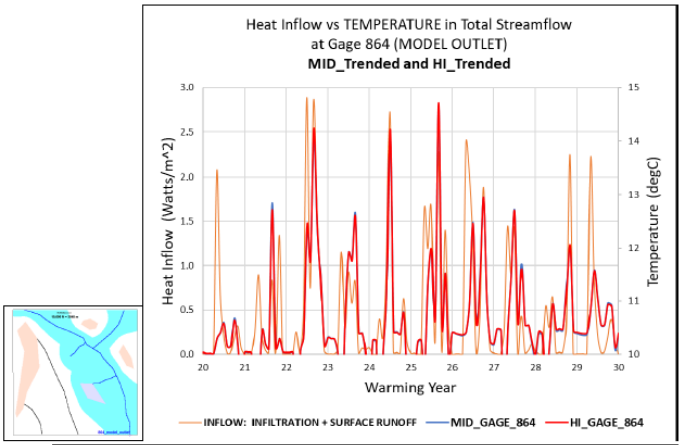

MID_Trended

LAGGED CORRELATION BETWEEN HEAT INFLOW and TEMPERATURE in TOTAL STREAMFLOW

Correlations stronger than 0.3 are highlighted; maximum gage correlation in boldface.

Monthly Lag	Gage 235	Gage 285	Gage 492	Gage 692	Gage 864
-1	0.010	0.014	0.008	0.000	0.002
0	**0.478**	**0.461**	**0.462**	**0.444**	**0.451**
1	0.250	0.246	0.239	0.240	0.242
2	0.305	0.301	0.297	0.303	0.304
3	0.140	0.142	0.142	0.164	0.160
4	0.198	0.201	0.200	0.221	0.217
5	-0.058	-0.061	-0.057	-0.024	-0.032
6	-0.207	-0.212	-0.205	-0.174	-0.182
AVERAGE 20-30 years	10.454	10.542	10.483	10.602	10.580
Ratio to Last Year of Spinup	1.043	1.051	1.047	1.059	1.056

HI_Trended

LAGGED CORRELATION BETWEEN HEAT INFLOW and TEMPERATURE in TOTAL STREAMFLOW

Correlations stronger than 0.3 are highlighted; maximum gage correlation in boldface.

Monthly Lag	Gage 235	Gage 285	Gage 492	Gage 692	Gage 864
-1	0.009	0.013	0.007	0.000	0.002
0	**0.479**	**0.468**	**0.468**	**0.450**	**0.457**
1	0.247	0.246	0.239	0.240	0.241
2	0.303	0.303	0.297	0.302	0.301
3	0.140	0.140	0.139	0.160	0.154
4	0.196	0.198	0.196	0.216	0.211
5	-0.053	-0.063	-0.058	-0.026	-0.034
6	-0.200	-0.213	-0.205	-0.175	-0.182
AVERAGE 21-30 years	10.456	10.562	10.502	10.612	10.591
Ratio to Last Year of Spinup	1.044	1.052	1.049	1.059	1.054

Figure S3.-11 f. (cont.): TEMPERATURE response (°C) along TOTAL STREAMFLOW pathway (including storm runoff) for MID_TRENDED and HI_TRENDED simulations. Graphs compare impulse heat flow in INFILTRATION to response TEMPERATURE in the pathway during the last 10 years of warming for contributing basins corresponding to headwater gage (235) and model outlet gage (864). Top table shows correlation coefficients between infiltration and total streamflow for five gage locations along stream network at different monthly time offsets (used in lag analysis). Bottom table shows change in total streamflow temperature between average for last year of spinup and last 10 years of warming for five gage locations along stream network (used in dampening analysis). Correlation coefficients greater than 0.3 are highlighted in yellow. Maximum value for each model version is in **bold** face; orange color demarcates pathway of interest.

Table S3-3. Lag results: Dominant time offsets between heat impulse and convective heat flow (Watts/m^2) or temperature (°C) response along pathways contributing to the 864 gage location.

Heat Flow to Heat Flow Pathway	Unit	Location	Model Version	Dominant Month Lags over warming (months with correlation > 0.3)	Month Lag with Maximum Correlation Value (correlation value)
From Inflow to Recharge to Water Table	Heat Flow [Watts/m^2]	Contributing Basin for model outlet (Gage 864)	MID_Trended	0 to 2	1 (0.667)
			HI_Trended	1 to 3	1 (0.515)
From Inflow to Direct Discharge to Streams	Heat Flow [Watts/m^2]	Contributing Basin for model outlet (Gage 864)	MID_Trended	2 to 3	3 (0.363)
			HI_Trended	1 to 3	1 (0.380)
From Inflow to Baseflow to Streams	Heat Flow [Watts/m^2]	Contributing Basin for model outlet (Gage 864)	MID_Trended	0 to 2	0 (0.582)
			HI_Trended	1 to 3	1 (0.445)
From Inflow to Total Streamflow	Heat Flow [Watts/m^2]	Gage at Downstream End of Lower Confluence (Gage 692)	MID_Trended	0 to 1	0 (0.964)
			HI_Trended	0	0 (0.962)
Heat Flow to Temperature Pathway	**Unit**	**Location**	**Model Version**	**Dominant Month Lags over warming (months with correlation > 0.3)**	**Month Lag with Maximum Correlation Value (correlation value)**
From Inflow to Flux-Weighted Temperature of Direct Discharge	Heat Flow [Watts/m^2] and Temperture (°C)	Contributing Basin for model outlet (Gage 864)	MID_Trended	no dominant months	3 (0.220)
			HI_Trended	no dominant months	4 (0.181)
From Inflow to Temperature of Total Streamflow	Heat Flow [Watts/m^2] and Temperture (°C)	Gage at Downstream End of Lower Confluence (Gage 692)	MID_Trended	0 to 2	0 (0.451)
			HI_Trended	0 to 2	0 (0.457)

Heat Flow Lags and Temperature Lags over Pathways from top of Unsaturated Zone.					
Heat Flow to Heat Flow Pathway	**Unit**	**Location**	**Model Version**	**Dominant Month Lags Over Warming** Months with Correlation Lag > 0.3	**Month Lag with Maximum Correlation Value** (correlation value)
From Inflow to Recharge to Water Table	Heat Flow [Watts/m^2]	Contributing Basin for	MID_Trended	0 to 2	1 (0.667)
		Model Outlet (Gage 864)	HI_Trended	1 to 3	1 (0.515)
From Inflow to Direct Discharge to Streams	Heat Flow [Watts/m^2]	Contributing Basin for	MID_Trended	2 to 3	3 (0.363)
		Model Outlet (Gage 864)	HI_Trended	1 to 3	1 (0.380)
From Inflow to Baseflow to Streams	Heat Flow [Watts/m^2]	Contributing Basin for	MID_Trended	0 to 2	0 (0.582)
		Model Outlet (Gage 864)	HI_Trended	1 to 3	1 (0.445)
From Inflow to Total Streamflow	Heat Flow [Watts/m^2]	Gage at Downstream End	MID_Trended	0 to 1	0 (0.964)
		of Lower Confluence (692)	HI_Trended	0	0 (0.962)
Heat Flow to Temperature Pathway	**Unit**	**Location**	**Model Version**	**Dominant Month Lags Over Warming: Months with Correlation Lag > 0.3**	**Month Lag with Maximum Correlation Value**
From Inflow to Flux-Weighted Temperature	Heat Flow [Watts/m^2]	Contributing Basin for	MID_Trended	no dominant months	3 (0.220)
of Direct Discharge	and Temperature [degC]	Model Outlet (Gage 864)	HI_Trended	no dominant months	4 (0.181)
From Inflow to Temperature	Heat Flow [Watts/m^2]	Gage at Downstream End	MID_Trended	0 to 2	0 (0.451)
of Total Streamflow	and Temperature [degC]	of Lower Confluence (692)	HI_Trended	0 to 2	0 (0.457)

The strength of the direct discharge correlation coefficients is roughly half as strong as those for the recharge coefficients (Table S3-3), indicating the time delay effect is more spread out for discharge. There is a similar pattern when comparing baseflow discharge to streams (the sum of direct groundwater discharge and groundwater runoff) and total streamflow (baseflow combined with storm runoff). The latter responds very quickly to thermal pulses at the land surface; the former shows some delay on the order of two months, more stretched out in time. Table S3-3 also contains lag findings between the heat impulse and the down-system temperature. The lag relation to groundwater discharge temperature is weak and drawn out in time, whereas, predictably, the total streamflow temperature response is quick (within 0-2 months) and relatively strong.

The dampening effect of pathways at the contributing basin scale manifests itself in several ways. Consider the relation of infiltrating heat flux to recharge heat flux averaged over the last 10 years of simulated warming. For both model versions, the reduction in the magnitude of the heat flow is between 14% and 20% (Figure S3-12a-b). The reduction of is much greater relative to the surface impulse in the case of the heat signal carried by baseflow to streams (Figure S3-12c-d). Leaving aside the anomalous headwater basin, it falls between 24% and 42% for both model versions. Another way to evaluate pathway dampening is by looking at how much of the increase in infiltrating heat flux due to warming is taken up by a pathway (Table S3-4). When average conditions for the last 10 years of warming are compared to the last year of spinup, results for the outlet gage show in the case of the **MID_TRENDED** simulation that recharging heat flux takes up 39% of the increase in infiltrating heat flow. The direct groundwater discharge pathways translate only 19% of the increase in infiltrating heat flux. That is, much of the generating heat impulse is stored, first, in the UZ and, then, in the groundwater system, manifesting itself as rising subsurface temperatures. This dampening effect is a bit more pronounced for the **HI_TRENDED** simulation, with only 38% and 12% of the infiltration warming increase taken up by recharge and direct heat discharge over the 30-year simulation period.

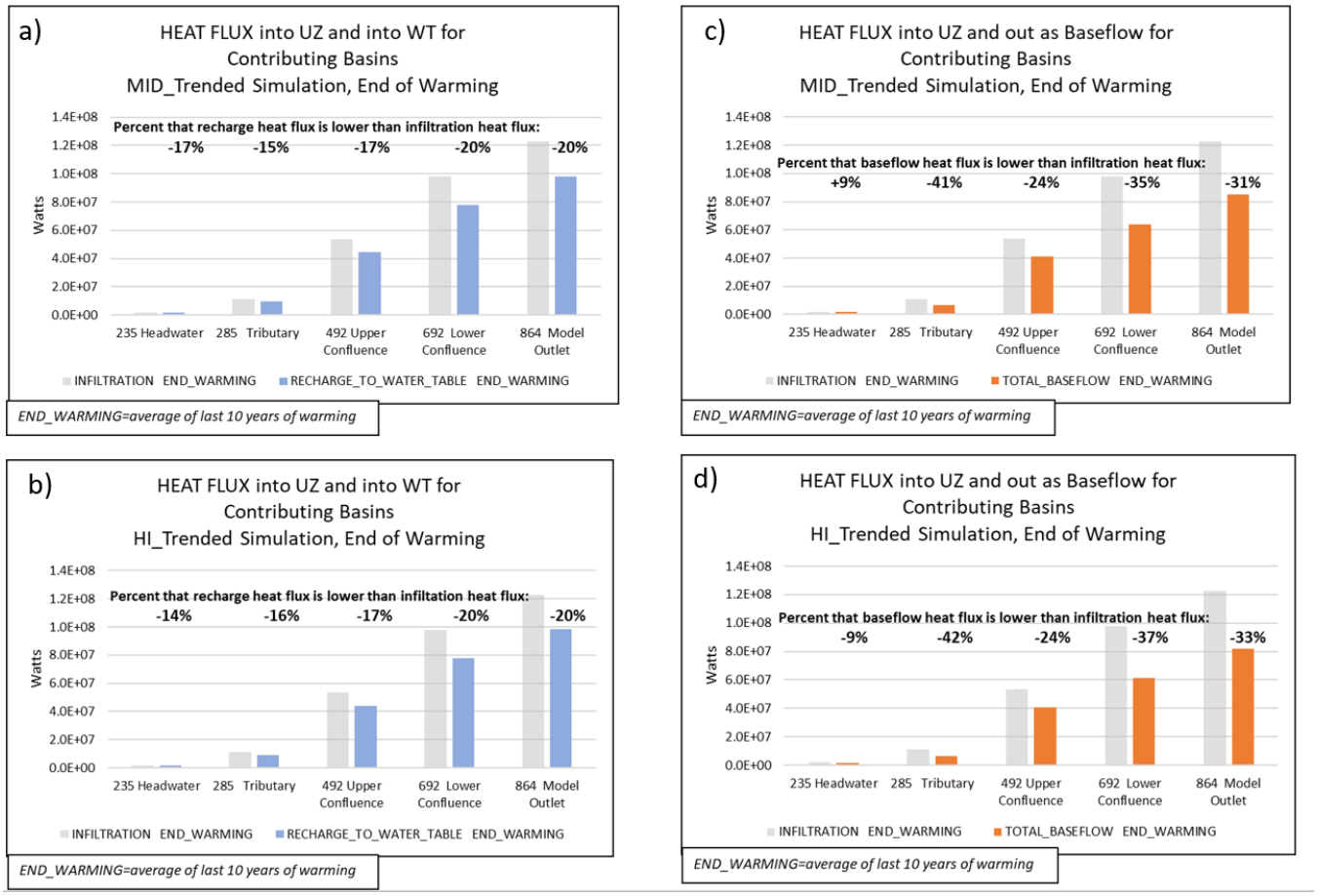

Figure S3-12. Percentage that convective heat pathway fluxes (watts) are dampened with respect to heat influx for contributing basins where fluxes are averaged over last 10 years of warming period; a) MID_TRENDED: Comparison of heat influx at top of unsaturated zone to recharging flux at water table; b) HI_TRENDED: Comparison of heat influx at top of unsaturated zone to recharging flux at water table; c) MID_TRENDED: Comparison of heat influx at top of unsaturated zone to baseflow discharge flux to streams and d) HI_TRENDED: Comparison of heat influx at top of unsaturated zone to baseflow discharge flux to streams.

Table S3-4. Ratio of increase in convective heat pathway fluxes (Watts) to increase in heat influx (Watts) for contributing basin corresponding to model outlet gage 864 for MID_TRENDED and HI_TRENDED simulations. Increases are calculated between end of spinup and end of warming.

Gage 864 model outlet	INFILTRATION heat flux (Watts) at end of spinup	INFILTRATION heat flux (Watts) at end of warming	RECHARGE heat flux (Watts) at end of spinup	RECHARGE heat flux (Watts) at end of warming	BASEFLOW DISCHARGE heat flux (Watts) at end of spinup	BASEFLOW DISCHARGE heat flux (Watts) at end of warming
MID_TRENDED	9.3×10^{7}	1.2×10^{7}	8.6×10^{7}	9.8×10^{7}	8.7×10^{7}	8.5×10^{7}
	Percent of infiltration		92.4%	79.7%	85.3%	69.4%
	Ratio of increases (delPATHWAY/delINFIL)			0.39		0.19
HI_TRENDED	9.3×10^{7}	1.2×10^{7}	8.8×10^{7}	9.9×10^{7}	7.8×10^{7}	8.2×10^{7}
	Percent of infiltration		93.7%	80.4%	83.9%	66.7%
	Ratio of increases (delPATHWAY/delINFIL)			0.38		0.12

Table S3-5 summarizes the pathway dampening that occurs between the last year of spinup and the last 10 years of warming in terms of heat flow at the outlet gage. The progression starts with a 31.3% average increase in the infiltrating heat flow within the basin contributing area due to imposed warming. The recharge calculated by the synthetic model passes along a fraction of that increase amounting for the two model versions to about a 13% increase relative to the spinup conditions. That is, the recharge only translates about 13/31 or 40% of the generating heat impulse. Further down-systems, there is a sharp drop off in the efficiency of heat propagation in the groundwater discharging directly to the stream reaches upgradient of the outlet gage. It amounts only to a 1.6% increase relative to spinup for the MID_TRENDED simulation and a 3.6% increase for the HI_TRENDED simulation (the difference is due to the large amount of competing riparian discharge in the first case). That is, the direct groundwater discharge only translates about 3/31 or approximately 10% of the generating heat impulse. There is comparatively less dampening when total baseflow discharge is substituted for direct groundwater discharge, but it still amounts to a small fraction of the starting impulse. Total streamflow at the outlet gage, because it incorporates storm runoff, experiences about a 12% average increase relative to spinup, showing a degree of dampening similar to that shown by recharge.

Table S3-5. Dampening of warming along watershed pathways: Attenuation of convective heat flow and temperature along pathways contributing to the 864 gage location for MID_TRENDED and HI_TRENDED simulations.

Heat Flow to Heat Flow Pathway	**Unit**	**Location**	**Model Version**	**Amplitude Percent Increase due to WARMING [from ratio of average value in last 10 years of WARMING to average value in last year of SPINUP]**
Infiltration	Heat Flow [Watts/m^2]	Uniform across Watershed	MID_ and HI_TRENDED	31.3%
Recharge to Water Table	Heat Flow [Watts/m^2]	Contributing Basin for model outlet (Gage 864)	MID_Trended	13.3%
			HI_Trended	12.7%
Direct Discharge to Streams	Heat Flow [Watts/m^2]	Contributing Basin for model outlet (Gage 864)	MID_Trended	1.6%
			HI_Trended	3.7%
Baseflow to Streams	Heat Flow [Watts/m^2]	Contributing Basin for model outlet (Gage 864)	MID_Trended	6.8%
			HI_Trended	4.4%
Total Streamflow	Heat Flow [Watts/m^2]	Gage at Downstream End of Lower Confluence (Gage 692)	MID_Trended	12.7%
			HI_Trended	11.1%
Heat Flow to Heat Temperature Pathway	**Unit**	**Location**	**Model Version**	**Amplitude Percent Increase due to WARMING** [from ratio of average value in last 10 years of WARMING to average value in last year of SPINUP]
Infiltration	Flux Weighted Temperature (^{o}C)	Uniform across Watershed	MID_ and HI_TRENDED	22.7%

Direct Discharge to Streams	Flux Weighted Temperature (°C)	Contributing Basin for model outlet (Gage 864)	MID_Trended	1.3%
			HI_Trended	1.3%
Total Streamflow	Flux Weighted Temperature (°C)	Gage at Model Outlet (Gage 864)	MID_Trended	5.6%
			HI_Trended	5.4%

A high degree of dampening is also evident in the temperature response to the infiltrating heat flow impulse for down-system pathways (Table S3-5). Recall that the flux-weighted temperature in the last year of spinup averages 9.97 °C and rises to an average of 12.23 for the last 10 years of warming, equivalent to a 23% increase (taking zero °C as the reference point). For both versions of UZ thickness, the direct groundwater discharge temperature increase amounts only to 1.3% over spinup conditions the corresponding total streamflow temperature increase is about 5.5%.

Simulation Results: Thermal Inertia Along Watershed Pathways

Excursion effects and flashiness, signal lags and trend dampening, are all aspects of thermal inertial along pathways. The hypothetical model shows how the inertial strength of the UZ and the full groundwater system acts on phase responses to heat fluctuations and on amplitude responses to heat trends originating at the top of the system. The blunting effect is opposed by the quick heat flows associated with groundwater runoff and, especially, with storm runoff. The distinct inertial strengths of watershed pathways combine to produce the complicated down-system baseflow and total streamflow responses.

This modeling exercise was limited to evaluating the response to a high-emission climate scenario over 30 years. If the warming were assumed to stabilize over a longer period, it is an open question at what rate the heat stored in the unsaturated zone and groundwater system would discharge as baseflow and streamflow. It is also in question to what extent the simulated excursions, lags and dampening are sensitive to assumed parameter values. Lower storage capacity, higher thermal conduction, lower thermal sorption, and higher UZ vertical hydraulic conductivity are levers to decrease thermal inertia. In other words, these parameters are all sources of uncertainty to be analyzed during a calibration process.

Any use of trade, firm, or product names is for descriptive purposes only and does not imply endorsement by the U.S. Government.

References

1. Morway, E.D.; Feinstein, D.T.; Hunt, R.J.; Healy, R.W. New capabilities in MT3D-USGS for Simulating Unsaturated-Zone Heat Transport. *Groundwater* **2022**. https://doi.org/10.1111/gwat.13256.
2. Feinstein, D.T.; Hunt, R.J.; Morway, E.D. Simulation of Heat Flow in a Synthetic Watershed: Lags and Dampening across Multiple Pathways under a Climate-Forcing Scenario. *Water* **2022**, *14*, 2810. https://doi.org/10.3390/w14182810.